The final publication is available at www.ascelibrary.org via:
https://ascelibrary.org/doi/abs/10.1061/%28ASCE%29ST.1943-541X.0002013

Validation of a Numerical Model for Prediction of Out-of-Plane Instability in Ductile Structural Walls under Concentric In-Plane Cyclic Loading

Farhad Dashti[1]; Rajesh P Dhakal[2]; and Stefano Pampanin[3]

ABSTRACT

Instability failure (also referred to as out-of-plane instability) has been observed in several experimental studies conducted on seismic performance of rectangular structural walls under in-plane loading. Observation of this failure pattern in some well-confined modern walls during the 2010 Chile and the 2011 Christchurch earthquakes has raised concerns on the reliability of current design code provisions. In this study, a numerical model composed of nonlinear shell-type finite elements has been proposed and validated for seismic performance prediction and simulation of out-of-plane instability failure in rectangular walls. The plane sections are not enforced to remain plane in the planar direction in this type of model, and the in-plane axial-flexure-shear interaction can be simulated without requiring any empirical adjustment. The element used in the model (curved shell element) has integration points along the thickness unlike flat shell elements in which integration is performed in one plane only. This element is consequently able to capture the variation of strain along the thickness and simulate the deformation in the out-of-plane direction. Experimental results of cantilever wall specimens which failed in out-of-plane mode are used for verification of the adopted modelling

[1] Research Engineer (Postdoctoral Researcher), UC Quake Centre, Dept. of Civil and Natural Resources Engineering, Univ. of Canterbury, Christchurch 8140, New Zealand. E-mail: farhad.dashti@pg.canterbury.ac.nz
[2] Professor, Dept. of Civil and Natural Resources Engineering, Univ. of Canterbury, Christchurch 8140, New Zealand. E-mail: rajesh.dhakal@canterbury.ac.nz
[3] Professor, Dept. of Civil and Natural Resources Engineering, Univ. of Canterbury, Christchurch 8140, New Zealand. E-mail: stefano.pampanin@canterbury.ac.nz

and analysis approach. The numerical model is found to be able to predict the trend of initiation, increase and recovery of out-of-plane deformation as well as the formation of out-of-plane instability that was observed during the tests. Development of this failure mechanism in the numerical model has been scrutinized using detailed response of the reinforcement and concrete elements positioned along the thickness of one of the specimens and at different stages of the failure mode. Also, the dependency of initiation and amount of the out-of-plane deformation on the maximum tensile strain developed in the longitudinal reinforcement during a specific loading cycle, and consequently all the parameters that influence its value (e.g. axial load, wall length, cyclic loading protocol, etc.), as well as wall thickness has been confirmed by a set of parametric studies conducted on the models developed for one of the wall specimens.

INTRODUCTION

In the recent earthquakes in Chile and New Zealand, lateral (out-of-plane) instability of reinforced concrete (RC) walls (Figure 1) was one of the failure patterns that raised concerns about performance of shear wall buildings designed using modern codes (Sritharan et al. 2014). Prior to the Chile earthquake, this failure mechanism had only been primarily observed in laboratory tests (Oesterle et al. 1976, Vallenas et al. 1979, Goodsir 1985, Johnson 2010). Out-of-plane buckling (also referred to as out-of-plane instability) of rectangular walls due to cyclic in-plane loads refers to buckling of an end region in a wall section where development of large tensile strains followed by a load reversal can result in exertion of large compression actions on reinforcing bars of a cracked section and provide an ideal situation for instability failure of the section.

Limited studies have been conducted on lateral stability of structural walls. The development of this failure mechanism was first investigated by Paulay and Goodsir (1985), following observations of out-of-plane instability in an experimental campaign conducted by Goodsir (1985). Based on the fundamental structural behaviour, the mechanics of out-of-plane

buckling was described in detail by Paulay and Priestley (1993) and recommendations were made for the prediction of the onset of out-of-plane instability. A major source of the instability was postulated to be the previously experienced tensile strain in a cracked wall section resulting in prevention of crack closure during load reversal. Chai and Elayer (1999) studied lateral stability of several reinforced concrete columns that were designed to represent boundary regions of rectangular structural walls, as shown in Figure 2. These columns were subjected to axial reversed cyclic tension and compression. Using axial strain versus out-of-plane displacement and axial strain versus axial force measurements, a generalised mechanism, as shown in Figure 3, was defined which describes the sequence of events resulting in development of out-of-plane instability in rectangular walls. Points *a-f* display different stages of the idealized column response and are briefly described in

Table 1.

Despite being one of the observed failure patterns of rectangular structural walls, numerical simulation of out-of-plane instability has been seldom attempted. Researchers have tried to simulate the out of plane instability by providing an initial imperfection (e.g. eccentricity in material properties) (Parra Torres 2016). In such cases, however, the outcome cannot be generic as the prediction greatly depends on the arbitrary value of the initial imperfection input to the loading. Moreover, the mechanism of out-of-plane instability failure is not clearly understood so far, and consequently the relevant design provisions are not backed up by strong research and clear understanding of the development of out-of-plane deformations in rectangular walls. In this study, a numerical modelling and finite element analysis approach that can simulate out-of-plane deformation and instability of rectangular walls is developed and experimentally verified. To the authors' knowledge, no finite element models reported in literature have been extensively verified for simulation of out-of-plane instability in rectangular walls under concentric in-plane cyclic loading, and the only attempt to model the wall out-of-plane buckling

of walls under monotonic loading using finite elements has been made by Attard et al. (1996). Hence, simulated results at different stages of the wall response are described in detail to establish beyond any doubt that it is possible to numerically predict the evolution of out-of-plane deformations and failure of walls due to out-of-plane instability under pure in-plane cyclic loading without making use of any artificial eccentricities.

FINITE ELEMENT MODEL

In this study, finite element analyses have been performed in DIANA9.4.4 (DIANA 2011) using curved shell elements. These elements are based on isoparametric degenerated-solid approach and have integration points along the thickness unlike flat shell elements in which integration is performed in one plane only. These elements are consequently able to capture variation of strain along the thickness and simulate the deformation in the out-of-plane direction. Two shell hypotheses are implemented in this approach (DIANA 2011): 1) Straight-normals: this hypothesis assumes that normals remain straight, but not necessarily normal to the reference surface. Transverse shear deformation is included according to the Mindlin-Reissner theory (Reissner 1945, Mindlin 1951). 2) Zero-normal-stress: it assumes that the normal stress component in the normal direction of a lamina basis is forced to zero.

The in-plane lamina strains ε_{xx}, ε_{yy} and γ_{xy} vary linearly across the thickness whereas the transverse shear strains γ_{xz} and γ_{yz} are forced to be constant in the thickness direction. Bar elements can be embedded inside the curved shell elements and in their accurate 3D positions. The Q20SH element, which is a four-node quadrilateral isoparametric curved shell element, is used in this study. The polynomials for the translations u and the rotations ϕ are expressed in Figure 4. Three-point integration scheme is considered along the thickness in which the integration points are located in the reference plane and at the two extremes of wall thickness (Figure 4).

During unloading and reloading of a cracked wall section, the compression is taken by the reinforcement only until the existing cracks in concrete close and concrete contributes to the load carrying capacity. This phenomenon is mainly controlled by residual strain of the reinforcement and is easily captured by the program using its path-dependent cyclic constitutive models. At this stage, the wall section is more likely to deform in a pattern that requires less energy. In this method, there is no need to make use of an artificial eccentricity that introduces a secondary bending moment, and out-of-plane deformation can be captured under pure in-plane loading through numerical computations and based on the energy consumed by different possible modes of deformation.

The behaviour of concrete elements is defined using the Total Strain Rotating Crack model. The equations proposed by Chang and Mander (1994) have been used to incorporate the compressive behaviour of confined and unconfined concrete and the tensile behaviour of concrete has been defined using the relations proposed by Belarbi and Hsu (1994). The reinforcing bars are modelled using embedded reinforcement approach available in the program with the properties defined using Menegotto and Pinto (1973) model. Bar buckling is not included in this constitutive model, hence the effect of bar buckling is neglected in the analysis conducted in this paper.

The size of the elements is determined based on a mesh sensitivity analysis. The numerical results are found not to be sensitive to the mesh size beyond a specific level of mesh refinement. On the other hand, the specimens with well-confined boundary regions are not very sensitive to fine mesh sizes. A typical mesh sensitivity analysis is presented for one of the specimens in the subsequent section.

The strain penetration effects that result in localized bond slip of the longitudinal reinforcement at the interface between wall and footing cannot be captured using this modeling approach. This phenomenon has been investigated by Zhao and Sritharan (2007) and Sritharan et al. (2000),

and its representation requires application of interface elements with appropriate hysteretic rules. As the fully bonded embedded bar approach has been used for representation of the reinforcement, the strain penetration effects would not have been captured if the foundation was simulated. Therefore, the footing is not simulated in this study, and the base of the wall is restricted against all six degrees of freedom. The loading line is restrained against movement in the out-of-plane direction using roller supports.

The displacement-controlled loading has been adopted using secant iterative method with Energy and Force as convergence norms. Geometric nonlinearity has been accounted for, and no artificial eccentricity has been implemented in the model to trigger out-of-plane buckling.

EXPERIMENTAL VERIFICATION

The model has been verified by the authors using experimental results of walls with different shear-span ratios which failed in different modes (Dashti 2017, Dashti et al. 2017). In this study, multiple wall tests reported in literature in which out-of-plane deformation was found to dominate the inelastic response are used for verification of the model capability in capturing out-of-plane instability.

Specimen R2 (Oesterle et al. 1976)

The first test used for the experimental verification is one of the cantilever wall specimens (R2) tested by Oesterle et al. (1976). This 1/3-scale specimen was a rectangular shaped wall with 4.0% vertical reinforcement concentrated within a distance of 190.5 mm (7.5 in.) from each end. The boundary element had confinement reinforcement in the lower 1.83 m (6 ft) of the boundary elements. Dimensions and reinforcement layout, loading history as well as the finite element model of the specimen are shown in Figure 5. The wall was subjected to in-plane loading only and the out-of-plane deformation was not triggered by any transverse

loading. The top nodes were constrained against translation in the out-of-plane direction (Figure 5d). The cantilever specimen was subjected to 39 displacement cycles at the top level as per the loading history shown in Figure 5c, and no axial load was applied. According to the test report (Oesterle et al. 1976), the specimen had a flexure-dominated response and its failure was accompanied by a large out-of-plane displacement of the compression zone within the lower 1.07 m (3 ft 6 in.) height as well as bar fracture and considerable crushing and loss of concrete.

Figure 6a compares the lateral load vs top displacement response of the model with the experimental measurements. The key milestones of the model response are also indicated in this figure. The magnified part of the figure shows the comparison for initial cycles where concrete cracking and reinforcement yielding initiate. As can be seen in this figure, the model could reasonably capture the specimen response in terms of elastic and inelastic behaviour, loading and unloading stiffness, peak strength, and cyclic degradation. Also, the milestones of the model response such as cracking and yielding points match well with the ones observed during the test. In particular, the analysis could capture the out-of-plane deformation in the compression boundary zone of the wall despite being subjected to pure in-plane action (Figure 6b). The Out-of-plane deformation initiated at Point F in the analysis and progressively increased during the following cycles.

Figure 7a displays the steel strain measurements of the specimen at wall base in comparison with the model predictions at the positive peak of selected drift cycles. Due to a gage malfunction the measurements were taken up to 0.56% drift in some parts and 1.1% drift at the tension boundary element. The nonlinear strain gradient along the length of the wall, which is usually neglected in simplified analysis methods, is predicted by the analysis with a relatively good agreement with the measured steel strain profile. Since the reinforcement elements are fully bonded in the analysis, the predicted strain profiles are identical for concrete and reinforcement. As shown in Figure 7a, the agreement between the predicted strain profile

of the wall section and strain measurements of the reinforcement in the test is reasonable. The strain profile at 1.1% drift level follows the same trend as the one at 0.56% drift level, but understandably with considerably greater strain values. The predicted neutral axis position matched well with test results as well. Figure 7b shows the vertical displacement of the mid-length node at the top level of the wall model indicating the wall elongation due to the residual strain developed in the reinforcement. Figure 8 displays the maximum out-of-plane displacement vs top in-plane displacement of the numerical model at both boundary zones.

The instability of the wall at different stages of loading due to out-of-plane deformation is further indicated in Figure 7b. As can be seen in this figure, Point F (initiation of out-of-plane deformation) corresponds to a sudden considerable drop in the elongation curve. The degradation reaches its maximum level as the out-of-plane deformation reaches its peak between Points F and G1 (Figure 8a). The wall moved up thereafter as the out-of-plane deformation recovered. This recovery was helped by the compressive stress sustained through the concrete elements located on the compression side of the buckled section. A similar trend is observed in the following cycles and with a considerable degradation and failure of the model at Point H (ultimate point). The degradation and failure of the model was due to the compressive stresses reaching the maximum strength of the confined concrete at the base and at the section with out-of-plane deformation. Initiation and development of out-of-plane deformation is described in more detail in the following sections.

According to the test report, the initial out-of-plane displacement was observed during Cycle 28, at 25.4 mm (1 in., 0.6% drift) deflection cycle after the 76.2 mm (3 in., 1.7% drift) cycles. The compression boundary element moved 6.4 mm (0.25 in.) out-of-plane at a point 1.1 m (3.5 ft) above the base. Although this out-of-plane deformation progressed further during subsequent cycles, the load carrying capacity of the wall remained stable. An omni-direction ball caster was placed against the face of each boundary element at 1.1 m (3.5 ft) above the

base. This simulated lateral support at approximately the first story height. The test was continued with the 101.6 mm (4 in., 2.2% drift) deflection cycle. Considerable out-of-plane deformation was observed during the 127 mm (5 in., 2.8% drift) deflection cycles, which progressed further until the strength dropped severely in the 6 in. deflection cycle.

In the analysis, flexural cracking initiated at 0.03% drift at a load of 51 kN and inclined cracks were observed at 0.14% drift at a load of 94 kN (Figure 6a, Points A&B). First yield of tension reinforcement occurred at 0.2% drift at a load of 121 kN and all the tension boundary element reinforcement yielded at 0.28% drift and a load of 132 kN (Figure 6a, Points C&D). The strain profile of the specimen at 0.28% drift (Figure 7) shows the neutral axis position is very close to the right end of the wall; thereby indicating that the unconfined concrete elements did not sustain much compression and most of the compressive stress was resisted by the confined boundary zone. The concrete in the right boundary zone reached the maximum strength at the end of 2.22% drift cycle (Figure 6a, Point E). While reversing from the positive peak drift, the compression boundary zone of the wall started to deform along the out-of-plane direction at a point 1.3 m (4.3 ft) above the base despite being subjected to pure in-plane action (Figure 6a, Point F). The height at which the out-of-plane initiated in the analysis (1.3m) is reasonably close to the one observed in the test (1.1m). This deformation increased as the drift reached -2.2%, and this phenomenon repeated during the subsequent drift cycles in both directions (Figure 6a, Points G1 and G2). It should be noted that at Points F, G1 and G2 which correspond to the initiation and development of out-of-plane instability, there is no degradation in the lateral load-top displacement response of the specimen as shown in Figure 6a while Figure 7b displays noticeable degradations corresponding to the initiation and development of out-of-plane deformation. This can be attributed to the fact that out of plane deformation resulted in earlier closure of the cracks in compression part of the section, contributing to load carrying capacity of the wall via redistributing the compression stresses. In other words, as a

result of the out-of-plane deformation, a considerable portion of the compression previously concentrated at the base (Point E) was transformed to the compression side of the section exhibiting out-of-plane deformation. At point H, due to the compressive stresses reaching the maximum strength of the confined concrete at the base and at the section with out-of-plane deformation, the wall became unstable.

As can be seen in Figure 8, the maximum out-of-plane deformation occurred alternately at the right and left boundary zones, whichever was under compression, and increased drastically after the 101.6 mm (4 in., 2.2% drift) cycle. The first 101.6 mm (4 in., 2.2% drift) cycle shows considerable recovery of the out-of-plane deformation along with the top displacement reaching the peak value of the cycle (Figure 8a, Point G1). The out-of-plane deformation increased along with the top displacement in the second and third cycles. Finally, the out-of-plane deformation became considerably larger during the first and second cycles of 127 mm (5 in. 2.8% drift) cycle resulting in instability of the model at Point H.

Mesh Size

Localization in finite element analysis has been thoroughly studied by Bažant and Oh (1983), Bazant and Planas (1997) and De Borst (1997), and the concrete post-peak tensile stress-strain response model as well as concrete compressive response are generally regularized to limit mesh sensitivity. Figure 9 displays the effect of the mesh size on response of the model for Specimen R2.

The change of mesh size from coarse to fine results in a consistent change, although not considerable, in the level of peak strength reached at each drift level (Figure 9a). However, response of the model with medium mesh size indicates a significant degradation at positive and negative peaks of 2.8% drift level. This level of degradation can be attributed to the increased level of out-of-plane deformations corresponding to the mesh size at 2.8% drift level when compared to the other mesh sizes (Figure 9b and Figure 9c). As can be seen in Figure 9b

and Figure 9c, the medium mesh size results in an out-of-plane deformation that generally lies between the coarse and fine mesh sizes with a decreasing trend as the mesh becomes finer. However, at large drift levels, the model with medium mesh size has larger out-of-plane displacements particularly at peak levels resulting in a significant degradation observed in Figure 9a. The value of out-of-plane deformation at each drift level seems to depend on the geometric configuration of the mesh elements, and apart from the degradation due to out-of-plane deformations, the mesh sensitivity analysis indicates a small difference in the model response. Therefore, as the localization does not seem to have a considerable effect on the model response, the material model regularization has not been addressed in this study.

Specimen 3 (Beattie 2004)

Development of out-of-plane deformation has been verified using experimental results of a singly reinforced slender wall tested by BRANZ research company (Beattie 2004), as well, for which the history of out-of-plane displacement was measured during the test. Figure 10 shows the cross section and reinforcement layout of this specimen. The longitudinal reinforcement is likely to be positioned with an eccentricity with respect to the section centreline in singly reinforced walls, which may influence their out-of-plane response. However, with the horizontal reinforcement placed at alternative sides of the vertical reinforcement (Figure 10), this eccentricity might have been very negligible in this specimen and has not been considered in the numerical simulation. The authors have investigated the effect of eccentricity of longitudinal reinforcement on out-of-plane response of singly reinforced walls in another study (Dashti et al. 2018a).

The simulated response is compared with the experimental measurements in Figure 11. The lateral load-top displacement response is reasonably predicted (Figure 11a) and the out-of-plane deformation pattern of the numerical model complies with the test observations (Figure 11b). The development of out-of-plane deformation at 2.5m above the floor at one end of the

panel and the out-of-plane displacement profile of the model are compared with the test results in Figure 11c and Figure 11d, respectively, which indicate the fast growth of out-of-plane deformation in the numerical model in comparison with the test results. As can be seen in Figure 11d, the out-of-plane displacement predicted by the numerical model is quite small during 1.0% drift level, which increases considerably during the subsequent drift levels leading to an out-of-plane displacement value that is 70% higher than the test measurements during 2.0% drift level. The increase in out-of-plane displacement made the model unstable and resulted in termination of the analysis before reaching -2.5% drift level (Figure 11a).

Specimen RWN (Johnson 2010)

Next, the test results of Specimen RWN (Johnson 2010) are used for further verification of the model. Figure 12 shows the cross section and reinforcement layout of this specimen. The lateral load was applied using an actuator located approximately 20 feet (6096 mm) above the wall/foundation interface and was transferred to the specimen with two steel channels, located on either side of the wall. Out-of-plane movement of the specimen was restrained by a lateral bracing and two structural wheels rolling inside the loading channels. The loading line in the numerical model was restrained against out-of-plane displacement using roller supports to represent this boundary condition. Figure 13 compares the numerical simulation with the experimental observations. The lateral load-top displacement response has been predicted quite reasonably except for the peak negative strength which is overestimated by the model. However, this discrepancy has been observed in some other numerical simulations of Specimen RWN such as Aaleti (2009) and Encina et al. (2016). According to the test report (Johnson 2010, Aaleti et al. 2013), Specimen RWN developed global, lateral instability of the boundary region comprised of the No. 5 and 6 bars (Figure 12) at 2.0% drift with the No. 9 bars in tension. Figure 13b compares the out-of-plane displacement profile of the model along the height of this boundary region with the test measurements at 2.0% drift level, and the deformation pattern of

the model is shown in Figure 13c. The model could reasonably predict the load-deflection response and the out-of-plane deformation which increased up to a certain level and recovered considerably at the peak displacement of the corresponding cycle.

Effect of Bar Buckling: Specimen PW4 (Birely 2013)

Inclusion of bar buckling in nonlinear response prediction of a wall would require either of the following approaches:

1- Using solid elements for both concrete and reinforcement to be able to mesh the cross section of a bar such that the strain variation along its cross section along with geometric nonlinearity can simulate bar buckling. This approach would immensely add numerical computational effort.

2- Using strain-based buckling models (e.g., Dhakal and Maekawa 2002) into the Menegotto-Pinto steel model. However, in the current modelling approach it is possible to track the strain-state of the main bars in the analysis and check if the strain corresponding to buckling-induced degradation of the material constitutive model (as per Dhakal and Maekawa model) has reached.

In order to address the effect of bar buckling on response of the model, a slender RC wall specimen PW4 tested by Birely (2013) was simulated as well. Figure 14 shows the geometry and reinforcement configuration of the specimen as well as its numerical vs experimental lateral load-top displacement response. According to Figure 14b, the cyclic response of the specimen was well captured by the analysis. The considerable drop of strength observed in the experimental response during the second cycle of 1.0% drift is due to extensive bar buckling and core concrete crushing. Out-of-plane deformation was also observed in the east boundary element of the wall. Since bar buckling was not taken into account in the analysis, the numerical model did not predict the loss of load carrying capacity. Therefore, the model was loaded up to 2.5% drift to investigate its out-of-plane response. The model exhibited very minor out-of-plane

deformation (less than 1 mm) at around zero displacement while unloading from +1.5% drift. This out-of-plane deformation increased with the increase in the applied drift level and reached a maximum value of 38 mm during the 2.5% drift level.

The model expectedly could not capture the main failure pattern of the specimen which was characterized by bar buckling. However, it could capture the out-of-plane deformation of the specimen which was observed in the test. According to the test report, the out-of-plane deformation had occurred earlier than the stage it was documented. Figure 15 displays the out-of-plane deformation pattern predicted by the numerical model.

The stress-strain curve of the reinforcing steel is captured for the extreme end longitudinal bars, and its propensity to buckling is scrutinized by using the strain-based buckling model proposed by Dhakal and Maekawa (2002a,b). This buckling model accounts for the effect of the axial stiffness of the transverse reinforcement in calculation of the buckling length. According to the detailing of the transverse reinforcement shown in Figure 14a, the extreme end longitudinal bars were restrained by transverse hoops of #2 located at 51 mm spacing which surrounded all the boundary zone bars. These hoops, extending over the whole length of the boundary zone, provided a very low amount of stiffness against buckling of the three extreme end bars, and according to the buckling model mentioned above, would result in a buckling length equal to four times the spacing of the transverse reinforcement. These bars would have a buckling length to bar diameter greater than 15, and the aforementioned buckling model results in considerable degradation of these bars' average compressive strength after yielding with 20% loss of compressive strength at a strain value of around -0.012. According to the test photo of the boundary region corresponding to the failure stage of the specimen, the buckling length extended over at least three confinement hoops. As can be seen in this figure, bar buckling had resulted in opening of the confining hoops leading to the loss of the confinement at the base of

the boundary region and an abrupt strength degradation due to bar buckling and concrete crushing of the compression boundary region.

The strain history of the extreme end bars of the numerical model showed that the strain value reached -0.0017 at initial stages of loading and, due to the accumulation of residual strain under cyclic loading, did not go below zero at higher drift levels even when the stress reached relatively high in compression. However, the stress-strain plot of the extreme end bars captured from the numerical model showed that the strain changed from +0.011 (at zero stress during unloading) to +0.001 (when the bar stress was maximum in compression) during the 1.0% drift cycle. In other words, the bar strains, despite being positive throughout the 1.0% drift cycle, decreased by about 0.01 mm/mm when the bar stress increased from zero to its maximum value in compression. As stated earlier, this amount of strain variation would result in the bars losing more than 20% of their compressive stress according to the Dhakal and Maekawa (2002b) buckling model. This is in line with the experimental response which shows an abrupt reduction of the wall strength after the buckling of bars.

DEVELOPMENT OF OUT-OF-PLANE DEFORMATION IN THE NUMERICAL MODEL

In order to scrutinize the sequence of events resulting in development of out-of-plane deformation in the numerical model, response of the numerical model generated for Specimen R2 is investigated in more detail in this section. For this purpose, behaviour of the reinforcement and concrete elements at the elevation corresponding to the maximum out-of-plane deformation and during the 101.6 mm (4 in., 2.2% drift) cycle is discussed. Figure 16a displays the lateral load vs top displacement response, and Figure 16b indicates the maximum out-of-plane displacement developed in the right and left boundary regions vs top displacement of the specimen corresponding to this specific cycle. Points a-f, shown in these figures, represent specific stages in out-of-plane response of the wall model. Deformation pattern of the wall at

these stages is illustrated using vertical and horizontal section cuts in Figure 17. The vertical strain gradients at Section 2-2, where the out-of-plane deformation initiated, and corresponding to the points noted above are shown in Figure 18. Wall faces as well as the loading direction are also displayed in these figures. The deformation pattern along the wall thickness and at both ends of the wall is shown graphically in each figure to further clarify the consistency of stress and strain gradients with the out-of-plane deformation. C and T stand for the compressive and tensile stresses applied to the reinforcement, respectively. The schematic crack opening is compatible with the strain gradient displayed in each figure and the stress gradients of reinforcement and concrete elements. These stress gradients that are used for interpretation of the material response along with development of out-of-plane deformation are indicated herein for Points a, b and c only (as shown in Figure 19), as these points typically represent the initiation, maximum and recovery of out-of-plane displacement (Figure 16b).

Point a corresponds to initiation of the out-of-plane deformation in the left boundary region. At this point, the model has already been unloaded from the top displacement of +101.6 mm (4 in., 2.2% drift), reversing towards -101.6 mm (4 in., 2.2% drift) and is sustaining the top displacement of 12.7 mm (0.3% drift). Figure 18a displays the considerable residual strain of the reinforcement and concrete elements remaining from the previous peak displacement. The previous tension side is under compressive stress at this point but the residual strain is large enough not to let the compression side experience a compressive strain. As can be seen in Figure 19a and Figure 19b, since the cracks have not closed at this stage, only the reinforcement elements carry the axial compression and the stress taken by the concrete elements is almost zero. The value of reinforcement compressive stress at this stage corresponds to onset of stiffness reduction (yielding in compression) in the cyclic constitutive model (Menegotto and Pinto 1973) defined for the reinforcement.

As shown in Figure 16, the out-of-plane deformation increases at the left boundary with increase of the top displacement until reaching Point b (-1.1% drift) and gradually decreases as the wall approaches Point c (-2.2% drift). At Point b, due to the out-of-plane deformation, strain profiles (Figure 18b) and stress profiles (Figure 19c and Figure 19d) of the concrete and reinforcement elements depend on their position along the wall thickness with the outer layers (concrete layers) experiencing the extreme values of axial strain. The out-of-plane deformation apparently closes the cracks at Face 2, resulting in development of compressive stresses in concrete elements at this face (as shown in Figure 19d). This crack closure can be considered as the main reason why the lateral load vs top displacement curve of the specimen does not show any strength degradation after development of out-of-plane deformation. The compressive stress taken by the reinforcement at this stage is significantly larger than the one corresponding to initiation of out-of-plane deformation (Point a).

Point c corresponds to -4in (-2.2% drift) top displacement. The maximum out-of-plane displacement at this point is about 40% less than the one at Point b (Figure 17c). As shown in Figure 18c, the strain sustained by tensile elements has increased considerably and accordingly the strain in the compression part has decreased. Also, the difference between strain profiles of Face1 and Face2 has decreased along with decrease of the out-of-plane deformation; indicating closure of cracks. The maximum compressive stress sustained by the reinforcement and concrete (Figure 19e and Figure 19f) is almost identical to the ones corresponding to Point b (Figure 19c and Figure 19d), while more concrete elements in the compression boundary region are subjected to increased compressive stress. This trend of variations in reinforcement and concrete compressive stresses indicates the fact that the out-of-plane deformation starts to recover (Figure 16b) as the crack closure results in development of a specific value of maximum compressive stress in concrete. With the contribution of concrete to load carrying capacity of the cracked wall section activated at this stage, further compression induced by larger lateral

displacement in the same direction is sustained by the inner face of the compression boundary zone (Concrete-Face 2, Figure 19f) with the maximum values of compressive stress not noticeably exceeding the one corresponding to the recovery onset of the out-of-plane deformation.

At Point d (zero base shear and -1.1% drift, Figure 16) the maximum displacement of the left boundary in the out-of-plane direction is still considerable (31 mm, Figure 17d). At this point, the out-of-plane deformation has started to develop in the other boundary zone (Figure 17d, Section 6-6). Separation of the strain profiles of concrete and reinforcing at the right boundary of the wall (Figure 18d) shows the initiation of out-of-plane deformation in that side of the wall as well. Further recovery of the previously formed out-of-plane deformation (Figure 17e, Section 4-4) is observed at Point e. At this point the top displacement applied to the wall is zero and the base shear is 70kN. Strain gradients (Figure 18e) indicate that out-of-plane deformations exist throughout the wall length. After Point e, the out-of-plane deformation increases rapidly (Figure 16b) at the right boundary zone, but the rate of increase of out-of-plane deformation reduces while reaching around 0.7% drift level and remains almost constant between 1.4% and 2.2% drift levels and increases again while approaching Point f corresponding to 2.8% drift (Figure 17f). At this stage, the compressive stress in Face 2 contributes to load carrying capacity of the wall and prevents the wall instability.

The strain and stress gradients indicated respectively in Figure 18 and Figure 19 clearly illustrate the combination of material response in a wall model at different stages of evolution of out-of-plane deformation. These figures show the variations of strain along the wall thickness which is a unique capability of the curved shell element; thereby enabling it to simulate out-of-plane deformations of walls under in-plane loading. Development of large compressive stresses in longitudinal reinforcement of a cracked wall boundary region can potentially lead to significant stiffness reduction in compression (compressive yielding) in these bars before crack

closure can activate contribution of concrete elements to the load carrying capacity of the section. This reduction of stiffness in compression (yielding in compression), if occurred along a sufficient height (effective buckling height) and length of the wall, can cause a considerable reduction of stiffness in its out-of-plane direction. The numerical model, making use of its ability to capture variation of strain along the thickness direction, would consequently choose to deform in this direction, which understandably requires less energy at this stage of cyclic loading. For the longitudinal reinforcing bars to yield in compression within the effective buckling height of the wall before crack closure during the load/strain reversals, the previously developed tensile strain in these bars must be evidently greater than two times their yield strain throughout this height.

The authors have experimentally investigated the evolution of out-of-plane deformation and the subsequent instability in rectangular walls in another study (Dashti et al. 2018b). The experimental observations regarding initiation, increase, and recovery of out-of-plane deformation, as well as the out-of-plane instability of rectangular walls, are in line with the mechanism predicted by the numerical model.

SENSITIVITY ANALYSIS OF THE MODEL

As noted above, evolution of out-of-plane deformation in the proposed numerical model is highly dependent on timely crack closure of a cracked wall section during reloading in the opposite direction. This crack closure is obviously controlled by the amount of residual tensile strain developed in the longitudinal reinforcement. If this strain exceeds a specific level (critical value), the induced out-of-plane deformation may become large enough to result in instability of the wall before redistribution of the compression stresses through crack closure can cause recovery of the out-of-plane deformation. However, for an increased wall thickness, this crack closure can happen earlier and larger residual strain would be required to cause out-of-plane instability. Figure 20 displays a schematic representation of this phenomenon. As can be seen

in this figure, there needs to be a critical value of tensile strain for a given wall thickness (t=b, Figure 20a) to provide ideal circumstances for development of out-of-plane instability. To prevent this, either the wall thickness should be increased (Figure 20b) to cause timely crack closure on one side of the wall and trigger contribution of concrete to load-carrying capacity of the section, or the tensile strain developed in the reinforcement should be prevented from reaching the critical value (Figure 20c). Consequently, wall thickness as well as all the parameters that can govern the maximum tensile strains developed in the boundary regions of walls (e.g. axial load, wall length, etc.) could be considered as the key parameters controlling out-of-plane instability of rectangular walls. It should be noted that some other parameters such as reinforcement ratio as well as the parameters known to influence bond stress between reinforcement and concrete (e.g. bar diameter) would potentially affect the crack/tensile strain distribution along the height of the boundary regions. These parameters can consequently alter the susceptibility of the wall to this mode of failure by producing strain localization (wide cracks) at the wall base and preventing the above mentioned compression yielding of the longitudinal reinforcement from occurring within sufficient height of the wall to create a global buckling (out-of-plane instability).

In this section, sensitivity of the numerical model to some parameters is evaluated. For this purpose, the effects of the maximum tensile strain imposed on the longitudinal reinforcement within a specific loading cycle, wall thickness and axial load on out-of-plane response of the numerical model generated for Specimen R2 has been investigated. These parameters are chosen because the available literature (Paulay and Priestley 1993, Chai and Elayer 1999) and the sequence of events predicted by the numerical model suggest that they have significant influence on out-of-plane deformation of rectangular walls under in-plane loading. It should be noted that this parametric study is not addressing all the parameters that can affect this mode of failure and is merely used to further verify the validity of the numerical model.

Residual strain of boundary region reinforcement

The effect of reinforcement strain on development of out-of-plane deformation can be investigated using single cycles of loading, unloading, and reloading in the opposite direction (Dashti et al. 2015). The numerical model of Specimen R2 was subjected to a relatively large lateral displacement which could generate a considerable tensile strain in the boundary region reinforcement. The wall was then unloaded and reloaded up to a significant drift level in the opposite direction. Checking this process on different initial loading amplitudes, the reinforcement strain corresponding to initiation of out-of-plane deformation was derived. Figure 21a displays the top displacement history corresponding to initiation of out-of-plane deformation, and Figure 21b shows the maximum out-of-plane displacement of the left boundary zone vs top displacement of the model. Figure 22 displays the axial strain vs out-of-plane displacement response of the boundary region reinforcement for both layers of reinforcement at the section where the out-of-plane displacement was the greatest. The deformation pattern along the wall thickness is shown graphically to further clarify the sequence of events (C and T stand for the compressive and tensile stresses applied to the reinforcement, respectively).

The same trend as observed in the idealized column specimens tested by Chai and Elayer (1999), shown in Figure 3, can be observed in Figure 22, and Points *a*-*d* correspond to the stages defined in Figure 3 and

Table 1. However, Point *e* does not correspond to concrete crushing. Although the model was subjected to -6.0% drift level, the axial strain at Point *e*, as shown in Figure 22, is only -0.0004 which is far away from the axial strain capacity of the boundary zone confined concrete. In other words, the crack closure starting from Point *d* is completed after the wall has been subjected to a considerably large drift, and the main load carrying capacity of the cracked section was provided by the reinforcement only until the magnitude of axial strain reached zero.

Also, the out-of-plane displacement predicted by the numerical model initiated at Point *c* (corresponding to a considerable loss of stiffness, i.e. compression yielding, at both layers of reinforcement), while the development trend of out-of-plane displacement proposed by Chai and Elayer (1999), shown in Figure 3, displays a gradual initiation of out-of-plane displacement due to the inherent eccentricity of the axial force, followed by compression yielding of the reinforcement closer to the applied axial force. The out-of-plane displacement would increase due to reduction of the transverse stiffness caused by this reinforcement yielding and would grow rapidly if a further increase in the axial compression results in compression yielding in the second layer of the reinforcement, as indicated by the near horizontal Path *c*-*d* (Figure 3). No eccentricities are accounted for in the numerical model and the out-of-plane deformation is mainly governed by compression yielding in the bars that are the main load carrying elements in a cracked wall section under compressive actions. The considerably abrupt increase of out-of-plane deformation in the numerical model when compared to the experimental measurements can be attributed to the sudden reduction of the transverse stiffness caused by this phenomenon. The eccentricities affecting out-of-plane response of the test specimens could be associated with material properties (e.g., yield strain of reinforcement), positioning of the longitudinal bars and axial load along the wall thickness.

The wall was loaded up to Point *a* (Figure 21a), which resulted in development of a tensile strain of 0.015 (equivalent to about $6\varepsilon_y$) in the extreme end longitudinal reinforcement (Figure 22) at the section where the out-of-plane displacement was the greatest. The wall was then subjected to a loading reversal, as shown in Figure 21a. Figure 22a shows a significant amount of residual strain developed in the extreme end reinforcement at Point *b*, where the reloading in the opposite direction starts and the axial stresses change sign (tension to compression). The strain at this stage is equal to 0.011 ($4.4\varepsilon_y$). The reinforcing bar undergoing compressive stresses with this amount of residual tensile strain can easily experience considerable yielding

in compression before the tensile strain reaches zero and cracks close. This compressive yielding, if developed along a sufficient height and length of the wall can provide ideal circumstances for deformation of the portion of the wall section under compressive actions in the direction that requires less energy, i.e., out-of-plane direction, until the cracks start closing in inner face of the out-of-plane displacement profile.

During Paths *o-a* and *a-b* (which correspond to loading and unloading stages, Figure 21a), the strain is identical in the two layers of reinforcement (Figure 22). As the out-of-plane deformation initiates at Point *c*, the reinforcement positioned in the inner face of the deformed section (referred to as Layer 1, Figure 22) undergoes a relatively bigger reloading in compression (recovering to smaller values of strain) for a given out-of-plane deformation when compared to the one in the outer face (referred to as Layer 2, Figure 22). The increase in out-of-plane displacement resulted in crack closure in the inner face at Point *d*, which in turn decreased the out-of-plane displacement during Path *d-e*, gradually reducing the difference between the axial strain values of the two layers of reinforcement. At Point *e*, the strain values at both layers of reinforcement are almost identical and are negative showing that the crack closure is almost complete with a rather minimal value of out-of-plane displacement.

Larger initial tensile strains were generated in the boundary region by applying a larger positive displacement in the model. Figure 23 displays the effect of this loading pattern on the response of the model. As can be seen in Figure 23a, the loading reversal after the model has been subjected to a larger displacement than the previous model resulted in considerable degradation starting from about -2.75% drift. This degradation was due to a continued increase in the out-of-plane displacement and eventual instability of the wall as the initial tensile strain was excessive and the subsequent compression did not result in the closure of the cracks and recovery of the out-of-plane displacement. This phenomenon is clearly shown in Figure 24. As

shown in this figure, unlike in Figure 22, the response follows Path *d-f*, which is in line with the trend proposed by Chai and Elayer (1999) (Figure 3,
Table 1). The initial tensile strain was equivalent to about $7.5\varepsilon_y$ in this case and the residual strain (Point *b*, Figure 24) was equivalent to about $5.7\varepsilon_y$.

The reinforcement response in these two cases (Figure 22 and Figure 24) indicates that the out-of-plane deformation tends to start when a considerable amount of compressive stress is developed in the reinforcing bars resulting in their compressive yielding before the crack closes and concrete restarts contributing to the wall's load carrying capacity. Larger tensile strains (Figure 24 compared with Figure 22) can readily lead to development of larger compressive stresses in the reinforcement prior to crack closure and trigger earlier initiation of reinforcement yielding in compression and consequently earlier deformation of the wall in the out-of-plane direction (Figure 23b compared with Figure 21b).

Figure 25 displays the strain history of the extreme end reinforcement of Specimen R2 subjected to the test load. This strain history is derived at 1.3m above the base, where the maximum out-of-plane deformation was observed, versus top displacement of the model. The points corresponding to initiation and development of out-of-plane deformation are shown in this figure. Figure 25a shows the level of strain reached by an extreme end reinforcement (ε_{sm}=0.0177) before initiation of out-of-plane deformation at Point F which is about seven times the yield strain and did not even reach the yield strain in compression when the wall was unloaded and reloaded in the opposite direction (Figure 25a, Point G1) while the strain corresponding to lower drift levels reached below zero at this stage. This strain is pretty close to the tensile strain of the reinforcement when the model was subjected to a single cycle and exhibited the first out-of-plane deformation (ε=0.015, Point *a*, Figure 22). The difference can be attributed to the effect of number of cycles in the test load which understandably increases the reinforcement strain. The maximum out-of-plane displacements corresponding to these two

cases are also consistent with the reinforcement strain in each case; i.e., 36mm for ε=0.015 (Figure 21b and Figure 22) and 75mm for ε_{sm}=0.0179 (Figure 8a and Figure 25a), indicating dependency of the out-of-plane response of the numerical model on the level of residual strain developed in the boundary region reinforcement.

Figure 25 shows the effect of out-of-plane deformation on strain distribution along the wall thickness, as well. The bar elements located at two different layers of reinforcement (Figure 25a and Figure 25b) undergo different strain histories after initiation of out-of-plane deformation at Point F, i.e., more compression in one layer (Figure 25a) rather than the other (Figure 25b). However, as also noted above, the reinforcement strain did not reach the yield strain after initiation of out-of-plane deformation even in the face undergoing more compression (Figure 25a, Point G1) until very large out-of-plane deformations corresponding to 2.8% drift level and failure at Point H.

The effect of residual strain of reinforcement on development of out-of-plane deformations is well discussed by Chai and Elayer (1999). Likewise, the initiation of out-of-plane displacement in the numerical model proved to be related to the level of residual strain developed in the boundary region reinforcement. It is shown that the exceedance of the residual strain above a specific level may result in the delay or prevention of crack closure when the same boundary region undergoes compression, which may cause out-of-plane instability of the wall due to the load being resisted by the reinforcement only for too long. Therefore, the sensitivity of the model response to residual strain of the longitudinal reinforcement is in agreement with the findings of the past experiments, which provides a further verification of the validity of the numerical model.

Wall Thickness

In order to study the effect of wall thickness on the model response, the model is analysed with different values for the wall thickness, as well. Figure 26a and Figure 26b display the lateral

load vs top displacement response and the maximum out-of-plane displacement at left boundary regions of the walls with increased thickness values, respectively. The thickness values are 1.5 times and 2.0 times the thickness of the test specimen.

As can be seen in Figure 26b, the increase in wall thickness considerably reduces the out-of-plane displacement of the wall. Also, the out-of-plane displacement recovers completely in the wall models with increased thickness when the wall reaches the peak displacement of each drift level. The effect of this parameter can be seen in Figure 26a, in which, unlike the test specimen, the walls with increased thickness do not exhibit any degradation. As out-of-plane deformation helps the cracks to close in thicker walls, an increase in wall thickness helps the walls to recover (i.e. straighten) even after experiencing a substantial residual tensile strain, which understandably results in more stable response of the wall, and the sensitivity of the model response to this parameter complies with this logic.

Axial Load

The wall model has been subjected to different levels of axial load, as well. Figure 27a and Figure 27b display the lateral load-top displacement response and the maximum out-of-plane displacement at right boundary regions of the walls with increased axial load ratios, respectively. Response of the models with axial load ratios ($\nu = N/f_c'A_c$) of 0.05 and 0.1 are compared with the one of the test specimen (axial load ratio = 0.0). The increase of axial load ratio to 0.05 has resulted in a considerable delay in initiation of out-of-plane deformation and consequently, a stable cyclic response without any degradation. Also, the out-of-plane deformations recovered completely at peak displacement levels of each drift level. However, the axial load ratio resulted in fast increase of the out-of-plane displacement when the specimen was unloaded from -2.8% drift. This fast increase in out-of-plane displacement of the right boundary region resulted in instability of the model and termination of the analysis. However, the model with axial load ratio of 0.1 did not exhibit any out-of-plane deformation (Figure 27b),

which can be due to the fact that the axial load prevents the bars from reaching the critical value of residual strain to trigger the out-of-plane deformation. The response of an extreme end bar under axial load ratio of 0.1 was compared with the one under zero axial load ratio. Although the increase in axial load ratio did not considerably influence the axial strain within the linear elastic stage of the reinforcement, its effect was quite pronounced in the post-yielding stage and resulted in about 15% decrease in the initially experienced axial strain. The decrease in axial strain resulting from the applied axial load along the compression reloading path can obviously affect the crack closure and prevent the out-of-plane displacements as the resulting crack opening is smaller than in the case without axial load. Therefore, an increase in axial load can delay or even prevent the onset of out-of-plane deformations by decreasing the residual tensile strain developed in the reinforcement. However, as out-of-plane deformation invariably increases the eccentricity of an axial load, it can produce additional destabilising P-Delta moment on the out-of-plane direction which accelerates the subsequent instability. In other words, the axial load can result in further increase of the out-of-plane displacement if it cannot prevent the initial tensile strain from reaching the critical value and the subsequent initiation of out-of-plane deformation.

It should be noted that the effects of axial load ratio on reinforced concrete structures are complex as it can easily change the failure mode (e.g. from flexure to shear or flexure-out of plane to flexure-concrete crushing), and it highly depends on other parameters like shear-span ratio. The strength degradation in the model with axial load ratio of 0.1 (Figure 27a) was due to concrete crushing under the applied moment and the increased axial load.

CONCLUSIONS

A finite element modelling and analysis approach using curved shell elements, which can reasonably simulate the trigger and development of out-of-plane deformation and also predict

failure of RC rectangular walls due to out-of-plane instability under in-plane loading (without any eccentricity), has been presented and experimentally verified in this paper.

The numerical model could predict the experimentally observed evolution of out-of-plane deformation within a loading cycle. The out-of-plane deformation was found to initiate when the load is reversed to zero, reach the maximum value at around zero percent drift and gradually recover during the loading phase in the opposite direction. The growth of out-of-plane deformation with the increase in the applied peak drift and the number of cycles per drift level, and consequently development of out-of-plane instability, was also successfully captured by the model. Furthermore, the predicted height corresponding to the maximum out-of-plane deformation was in good agreement with the experimental observations. However, the out-of-plane deformation progressed faster in the numerical model than that observed in the tests.

Strain and stress gradients of the reinforcement and concrete elements at different stages of loading were used to scrutinize the evolution of out-of-plane deformation in the numerical model, which was found to comprise of the following two stages:

1- Development of large tensile strains in the longitudinal reinforcement of a wall model can readily lead to generation of significant compressive stresses in these bars during loading reversal and, according to the cyclic constitutive models defined for reinforcing steel, result in considerable reduction of their axial compressive stiffness. This reduction of stiffness in compression (yielding in compression), if occurred along a sufficient height and length of the wall, can cause a considerable reduction of stiffness in its out-of-plane direction. The numerical model, making use of its ability to capture the variation of strain along the thickness direction, would consequently choose to deform in this direction, which understandably requires less energy at this stage of cyclic loading.

2- The initially induced axial strains of the extreme integration points along the wall thickness and at one of the two wall faces would change from tension to compression (representing crack closure) at the elevation corresponding to the maximum out-of-plane deformation. This would activate load carrying capacity of concrete elements and result in recovery of the out-of-plane deformation (i.e. straightening of the wall) as the loading reversal is continued. This is the reason why the out-of-plane deformation, if insufficient to trigger out-of-plane instability, does not cause any strength degradation in the lateral load-top displacement response of the model.

The mechanism noted above would be affected by initial tensile strain induced in the longitudinal reinforcement; thereby any parameters affecting this strain (e.g. axial load, wall length, etc.) as well as wall thickness. As further verification of the model validity, the numerical model was evaluated for its sensitivity to these parameters and is found to exhibit logical responses to these variations.

Larger tensile strains were found to lead to development of larger compressive stresses in the reinforcement upon load reversal; thereby making it more likely for the reinforcement to yield in compression prior to crack closure, which consequently results in larger out-of-plane deformation. If the induced tensile strains are large enough, this could result in out-of-plane instability of the wall model before crack closure could contribute to recovery of the out-of-plane deformation. Such instability was found to cause a significant strength reduction in load-displacement response of the wall model. This effect is further supported by the postulations and findings provided by other researchers which are based on experimental observations.

An increase in wall thickness was found to reduce the maximum amount of out-of-plane deformations. Also, the out-of-plane displacement recovered completely in the wall models with increased thickness when the wall reached the peak displacement of each drift level.

The effect of axial load was also investigated due to its potential contribution to both prevention of out-of-plane deformation by reducing the residual strain of the longitudinal reinforcement and accelerating the progression of out-of-plane instability by introducing further destabilizing moment through P-Delta effect. This contradictory dual role of axial load on this mode of failure was also successfully captured by the numerical model.

The sequence of events resulting in formation of out-of-plane instability in the numerical model was in good agreement with the mechanism experimentally derived and described by Chai and Elayer (1999). The effects of eccentricities along the wall thickness associated with material properties, positioning of the longitudinal reinforcement and loading, which are known to potentially affect the development of this failure pattern, were not incorporated in the numerical model to avoid dependency of the prediction on some quantitatively and qualitatively uncertain values. These eccentricities are likely to prevent development of identical tensile and compressive strains across the wall thickness. Consequently, the onset and increase of out-of-plane deformation was rather abrupt in the numerical model due to simultaneous compressive yielding in both layers of the longitudinal reinforcement. This rapid progression of the out-of-plane deformation does not conform to the mechanism proposed by Chai and Elayer (1999) and to the other experimental observations as the eccentricities mentioned above do obviously exist in reality.

REFERENCES

Aaleti, S. R. (2009). Behavior of rectangular concrete walls subjected to simulated seismic loading, Iowa State University. PhD**,** 249.

Attard, M. M., N. Minh and S. J. Foster (1996). "Finite element analysis of out-of-plane buckling of reinforced concrete walls." *Computers & structures* 61(6), 1037-1042.

Bažant, Z. P. and B. H. Oh (1983). "Crack band theory for fracture of concrete." *Matériaux et construction* 16(3), 155-177.

Bazant, Z. P. and J. Planas (1997). Fracture and size effect in concrete and other quasibrittle materials, CRC press.

Beattie, G. J. (2004). Design of Slender Precast Concrete Wall Panels – Experimental Testing. BRANZ Study Report SR 129, BRANZ Ltd, Judgeford, New Zealand.

Belarbi, A. and T. T. Hsu (1994). "Constitutive laws of concrete in tension and reinforcing bars stiffened by concrete." *ACI Structural Journal* 91(4).

Birely, A. C. (2013). Seismic Performance of Slender Reinforced Concrete Structural Walls, University of Washington. PhD**,** 983.

Chai, Y. H. and D. T. Elayer (1999). "Lateral stability of reinforced concrete columns under axial reversed cyclic tension and compression." *ACI Structural Journal* 96(5), 780-789.

Chang, G. and J. B. Mander (1994). Seismic energy based fatigue damage analysis of bridge columns: Part I-Evaluation of seismic capacity, National Center for Earthquake Engineering Research Buffalo, NY.

Dashti, F. (2017). Out-of-plane Instability of Rectangular Reinforced Concrete Walls Under In-plane Loading. Department of Civil and Natural Resources Engineering, University of Canterbury. PhD**,** 295.

Dashti, F., R. Dhakal and S. Pampanin (2015). Development of out-of-plane instability in rectangular RC structural walls 2015 NZSEE Conference, Rotorua, New Zealand, New Zealand Society for Earthquake Engineering.

Dashti, F., R. P. Dhakal and S. Pampanin (2017). "Numerical Modeling of Rectangular Reinforced Concrete Structural Walls." *Journal of structural engineering* 143(6). DOI: 10.1061/(ASCE)ST.1943-541X.0001729.

Dashti, F., R. P. Dhakal and S. Pampanin (2018a). "Blind prediction of in-plane and out-of-plane responses for a thin singly reinforced concrete flanged wall specimen." *Bulletin of Earthquake Engineering* 16(1), 427–458. DOI: 10.1007/s10518-017-0211-x.

Dashti, F., R. P. Dhakal and S. Pampanin (2018b). "Evolution of out-of-plane deformation and subsequent instability in rectangular RC walls under in-plane cyclic loading: Experimental observation." *Earthquake Engineering and Structural Dynamics*, DOI: 10.1002/eqe.3115.

De Borst, R. (1997). "Some recent developments in computational modelling of concrete fracture." *International journal of fracture* 86(1-2), 5-36.

Dhakal, R. P. and K. Maekawa (2002b). "Reinforcement stability and fracture of cover concrete in reinforced concrete members." *Journal of structural engineering* 128(10), 1253-1262.

DIANA, T. (2011). Finite Element Analysis User's Manual - Release 9.4.4, TNO DIANA.

Encina, E., Y. Lu and R. Henry (2016). "Axial elongation in ductile reinforced concrete walls." *Bulletin of the New Zealand Society for Earthquake Engineering* 49(4), 305-318.

Goodsir, W. J. (1985). The design of coupled frame-wall structures for seismic actions, University of Canterbury. PhD.

Johnson, B. (2010). Anchorage detailing effects on lateral deformation components of R/C shear walls, Master Thesis, University of Minnesota.

Kam, W. Y., S. Pampanin and K. Elwood (2011). "Seismic performance of reinforced concrete buildings in the 22 February Christchurch (Lyttelton) earthquake." *Bulletin of the New Zealand Society for Earthquake Engineering* 44(4), 239-278.

Menegotto, M. and P. Pinto (1973). Method of Analysis for Cyclically Loaded Reinforced Concrete Plane Frames Including Changes in Geometry and Non-elastic Behavior of Elements Under Combined Normal Force and Bending. IABSE Symposium on the Resistance and Ultimate Deformability of Structures Acted on by Well-Defined Repeated Loads, Lisbon, Association internationale des ponts et charpentes.

Mindlin, R. D. (1951). "Influence of rotary inertia and shear on flexural motions of isotropic, elastic plates." *J. of Appl. Mech.* 18, 31-38.

Oesterle, R., A. Fiorato, L. Johal, J. Carpenter, H. Russell and W. Corley (1976). "Earthquake resistant structural walls-tests of isolated walls." Research and Development Construction Technology Laboratories, Portland Cement Association.

Parra Torres, P. F. (2016). Stability of Reinforced Concrete Wall Boundaries, University of California, Berkeley.

PhD, 219.

Paulay, T. and W. Goodsir (1985). "The ductility of structural walls." *Bulletin of the New Zealand Society for Earthquake Engineering* 18(3), 250-269.

Paulay, T. and M. Priestley (1993). "Stability of ductile structural walls." *ACI Structural Journal* 90(4), 385-392.

Reissner, E. (1945). "The effect of transverse shear deformation on the bending of elastic plates." *Journal of applied Mechanics* 12, 69-77.

Sritharan, S., K. Beyer, R. S. Henry, Y. Chai, M. Kowalsky and D. Bull (2014). "Understanding poor seismic performance of concrete walls and design implications." *Earthquake Spectra* 30(1), 307-334.

Sritharan, S., M. J. Nigel Priestley and F. Seible (2000). "Nonlinear finite element analyses of concrete bridge joint systems subjected to seismic actions." *Finite Elements in Analysis and Design* 36(3–4), 215-233. DOI: http://dx.doi.org/10.1016/S0168-874X(00)00034-2.

Vallenas, J. M., V. V. Bertero and E. P. Popov (1979). Hysteretic behaviour of reinforced concrete structural walls. Report no. UCB/EERC-79/20, Earthquake Engineering Research Center, University of California, Berkeley.

Wallace, J. (2012). "Behavior, design, and modeling of structural walls and coupling beams — Lessons from recent laboratory tests and earthquakes." *International Journal of Concrete Structures and Materials* 6(1), 3-18. DOI: 10.1007/s40069-012-0001-4.

Zhao, J. and S. Sritharan (2007). "Modeling of strain penetration effects in fiber-based analysis of reinforced concrete structures." *ACI Structural Journal* 104(2), 133-141.

Table 1. Behavior of wall end-region under the loading cycle shown in Figure 3

Loading stage	Path	Key features
Loading	o-a	Large tensile strain
Unloading	a-b	Elastic strain recovery mainly in reinforcing steel
Reloading	b-c	Reloading in compression on the cracked concrete column accompanied by an out-of-plane displacement; yielding of the reinforcement closer to the applied axial force resulting in a reduced transverse stiffness of the column and an increased out-of-plane displacement.
	c-d	Compression yielding in the second layer of the reinforcement, and a rapid increase in the out-of-plane displacement
	d-e	Closure of cracks at Point d and decrease of out-of-plane displacement and increase of out-of-plane displacement after significant compressive strain is developed in the compressed concrete
	d-f	An excessive crack opening where subsequent compression would not result in the closure of the cracks but a continued increase in the out-of-plane displacement and eventual buckling of the column

Figure 1. Out-of-plane instability of well-confined wall (2011 Christchurch earthquake) (reprinted from Kam et al. 2011, with permission from the New Zealand Society of Earthquake Engineering Inc)

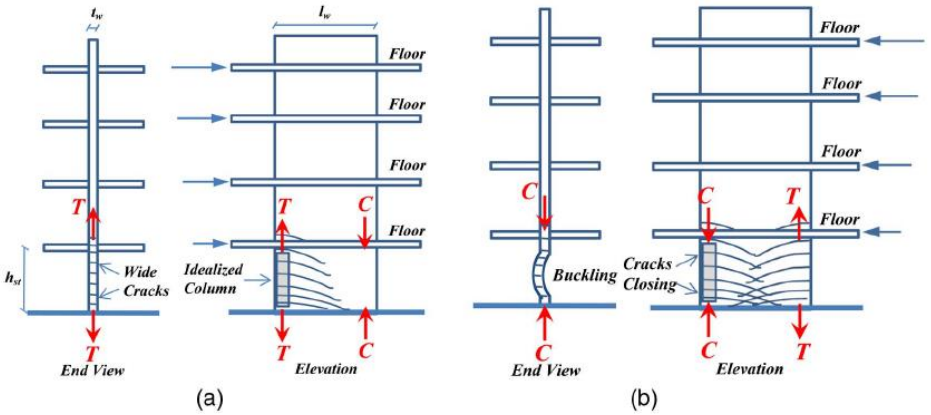

Figure 2. Idealization of reinforced concrete wall in end regions (adapted from Chai and Elayer 1999, with permission from the American Concrete Institute): (a) opening of cracks under tension cycle; and (b) closing of cracks under compression cycle

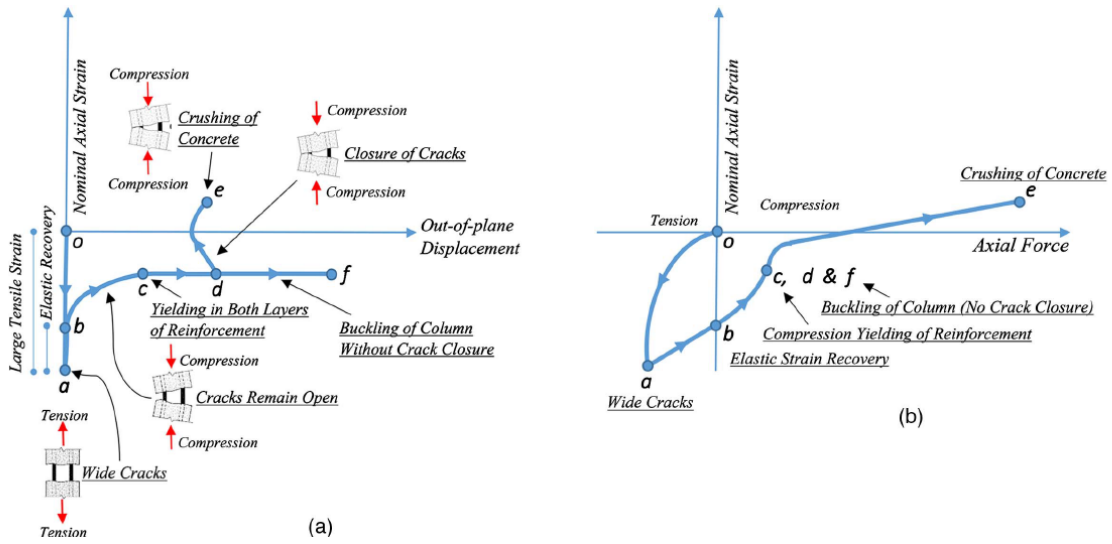

Figure 3. Axial reversed cyclic response of reinforced concrete column (adapted from Chai and Elayer 1999, with permission from the American Concrete Institute): (a) nominal axial strain versus out-of-plane displacement; and (b) nominal axial strain versus axial force

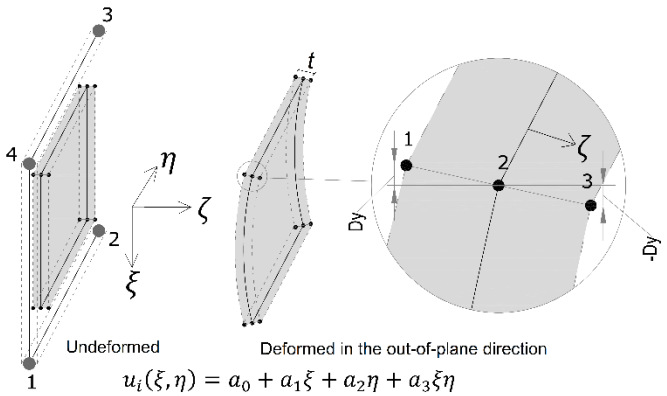

$$u_i(\xi,\eta) = a_0 + a_1\xi + a_2\eta + a_3\xi\eta$$
$$\theta_i(\xi,\eta) = b_0 + b_1\xi + b_2\eta + b_3\xi\eta$$

Figure 4. Four-node curved shell element with three-point integration scheme across the thickness

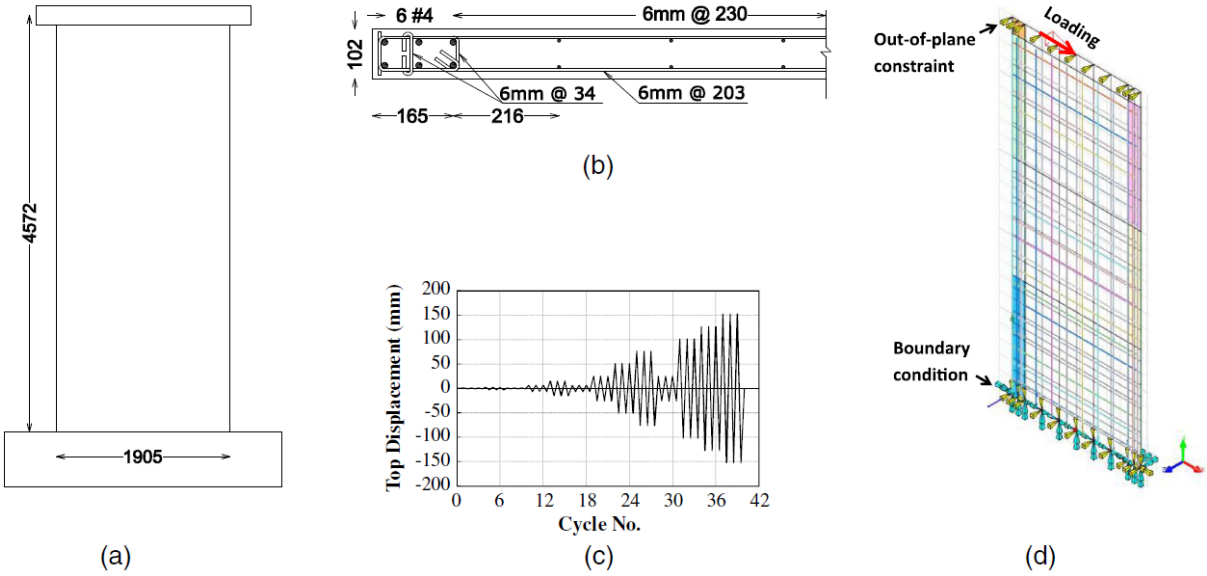

Figure 5. Specimen R2: (a) dimensions; (b) cross section; (c) loading history; (d) finite element model (all dimensions in mm)

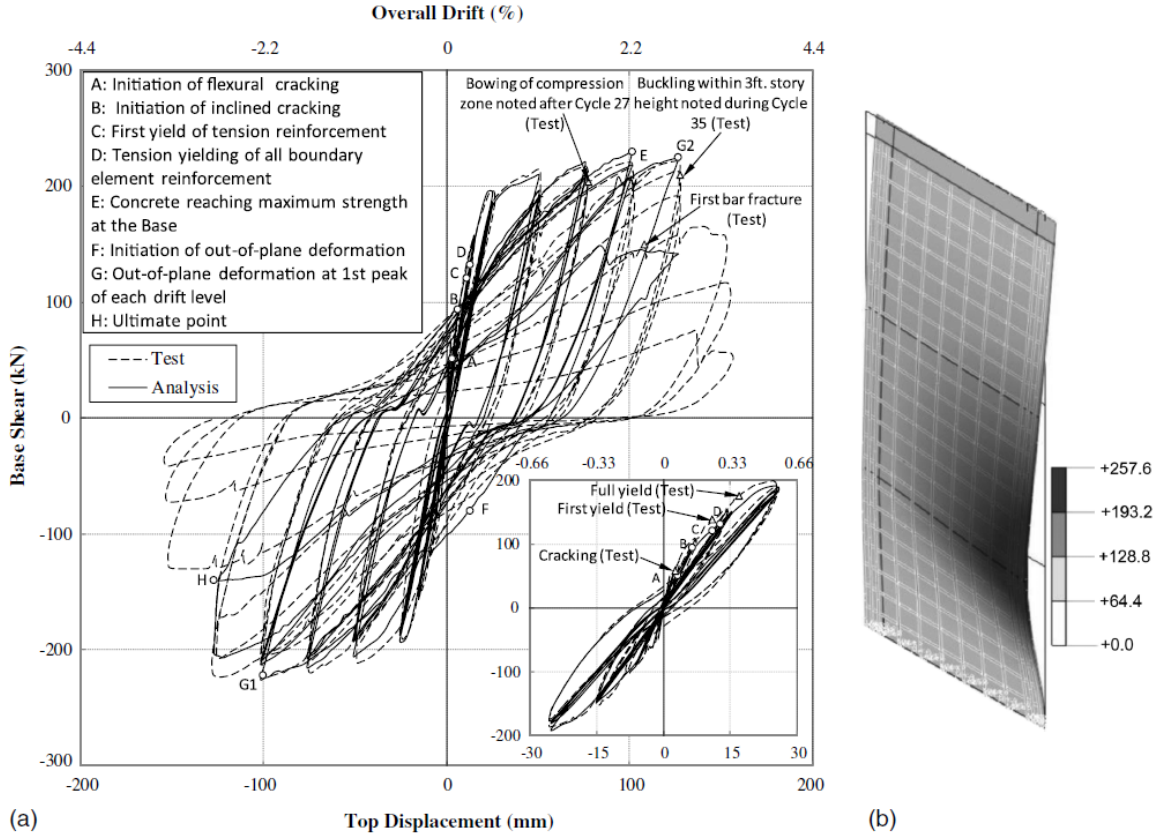

Figure 6. Response of the model: (a) lateral load vs top displacement response; (b) out-of-plane deformation corresponding to the 2nd 2.2% drift cycle

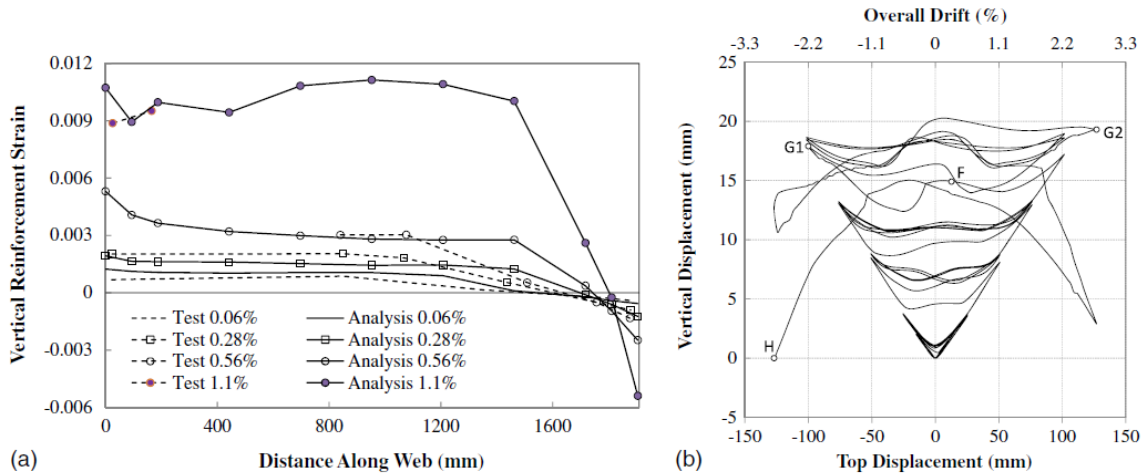

Figure 7: (a)Variation of the vertical reinforcement strain along the wall length; (b) vertical displacement (uplifting due to plastic hinge elongation) at mid-length of the specimen – numerical prediction

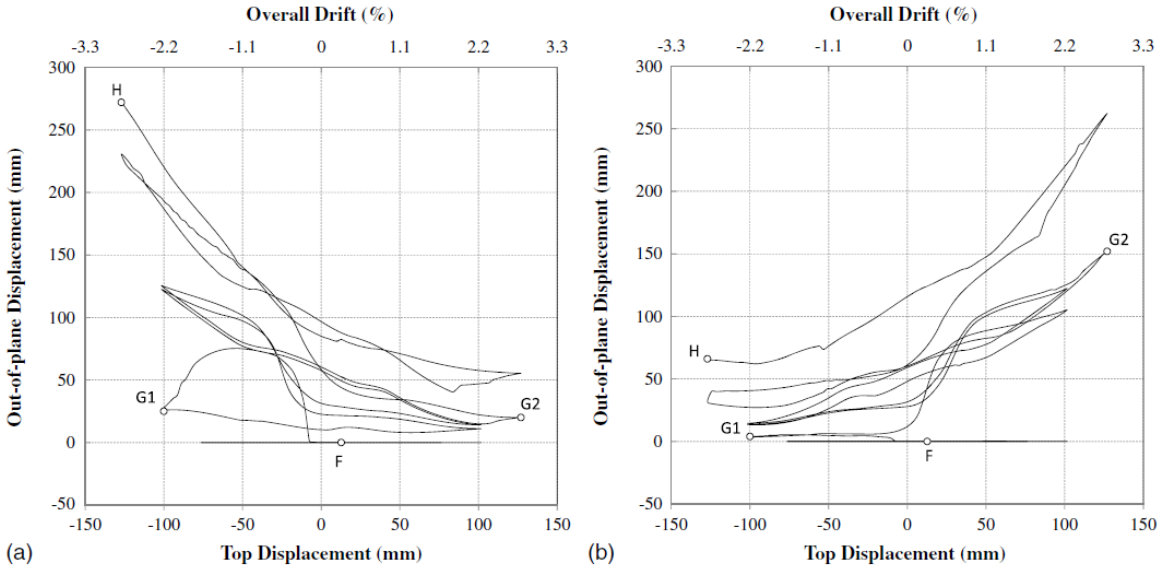

Figure 8. Numerical prediction of maximum out-of-plane displacement: (a) left boundary zone; (b) right boundary zone

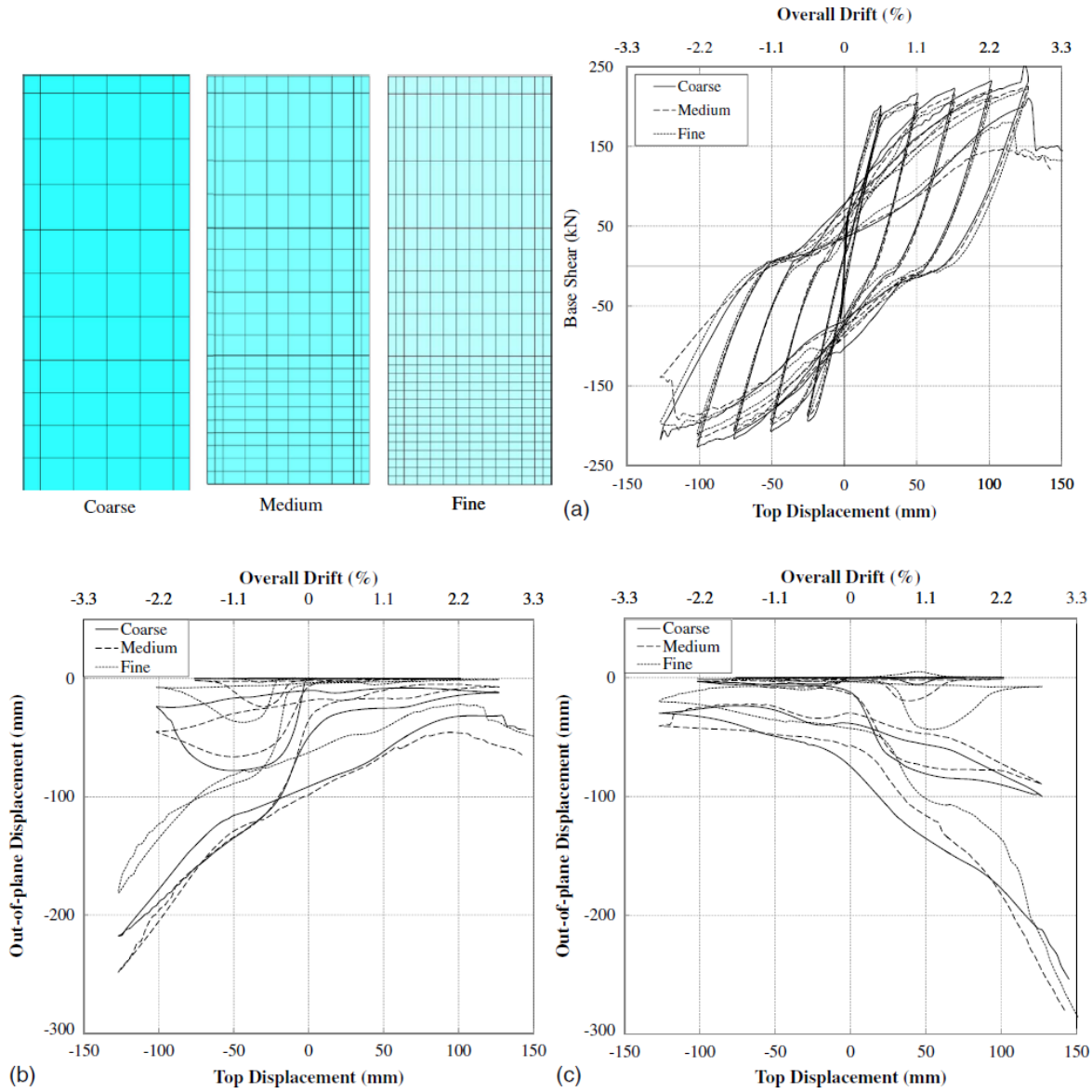

Figure 9. Mesh sensitivity of the model: (a) lateral load-top displacement response; (b) maximum out-of-plane displacement in the left boundary region; (c) maximum out-of-plane displacement in the right boundary region

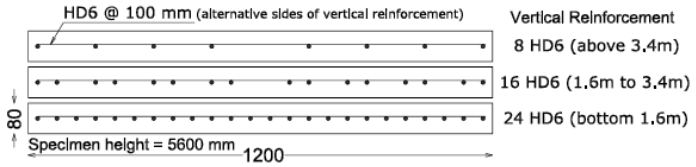

Figure 10. Cross section and reinforcement layout of Specimen 3

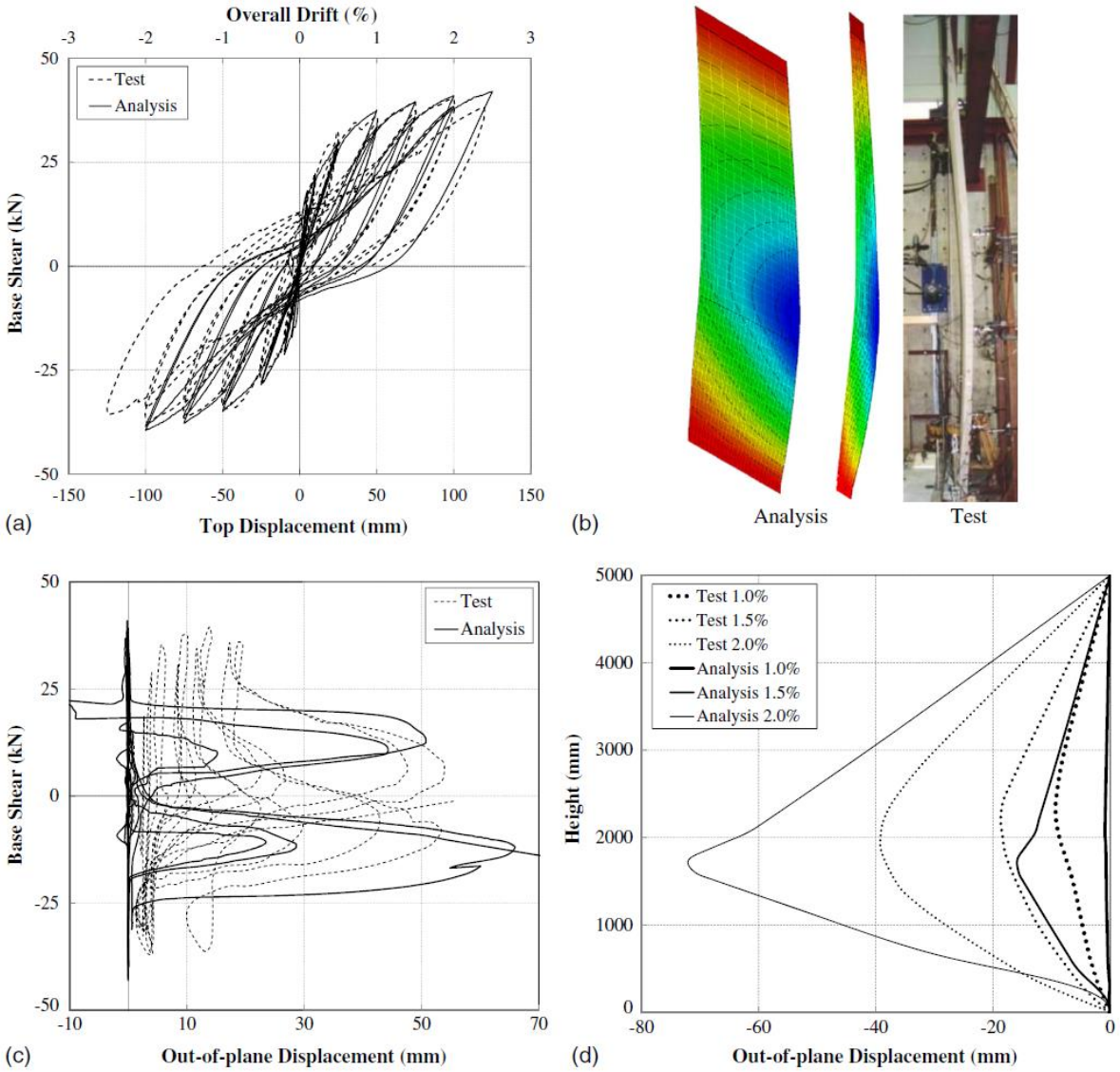

Figure 11. Simulation of out-of-plane instability in Specimen 3: (a) lateral load vs top displacement response; (b) simulated vs experimental out-of-plane deformation (test photo from Beattie 2004); (c) out-of-plane displacement vs base shear at 2.5m above the base; (d) out-of-plane displacement profile along the height of the wall at different drift levels

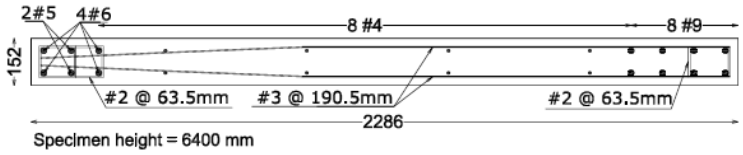

Figure 12. Cross section and reinforcement layout of RWN

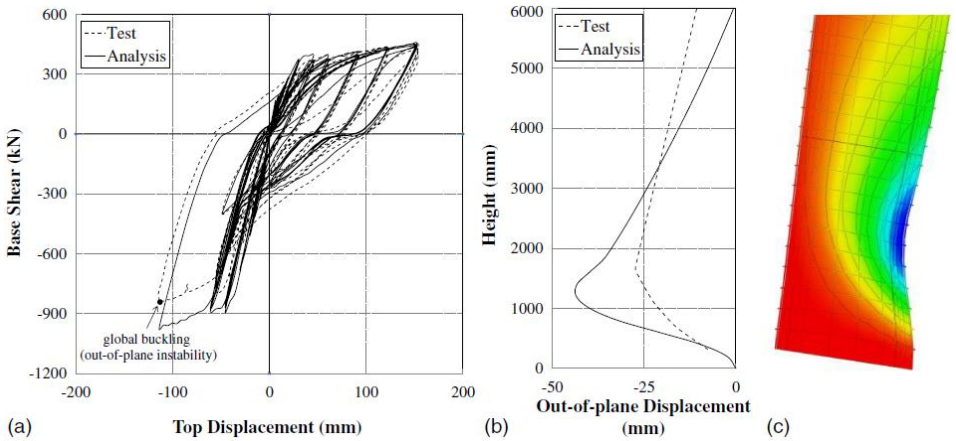

Figure 13. Simulation of out-of-plane instability in S pecimen RWN: (a) lateral load vs top displacement response; (b) out-of-plane displacement profile along the height of the wall following 2.5% drift level; (c) simulated out-of-plane instability

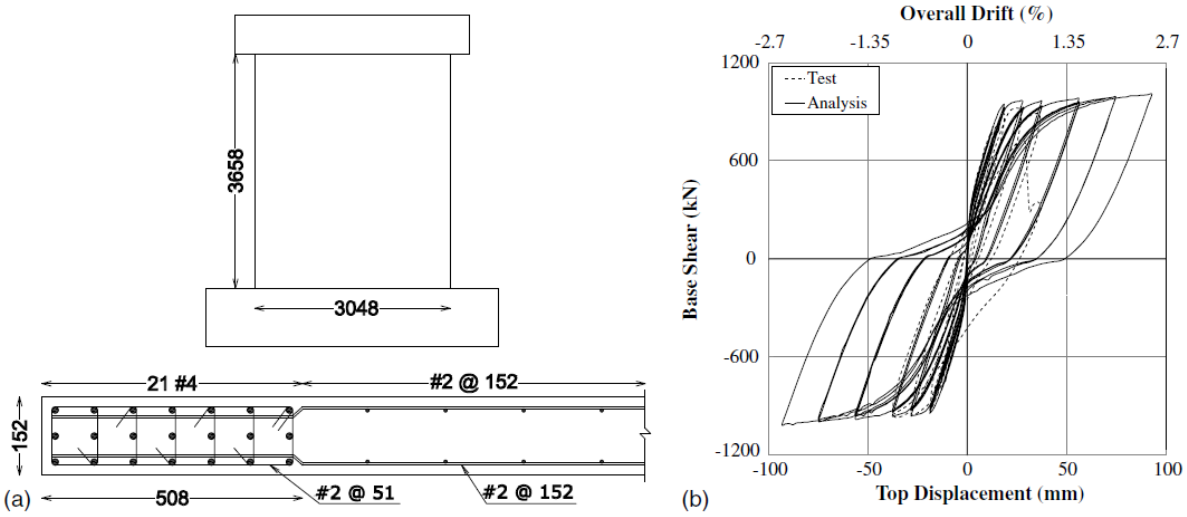

Figure 14. Specimen PW4: (a) geometry and reinforcement configuration; (b) lateral load-top displacement response

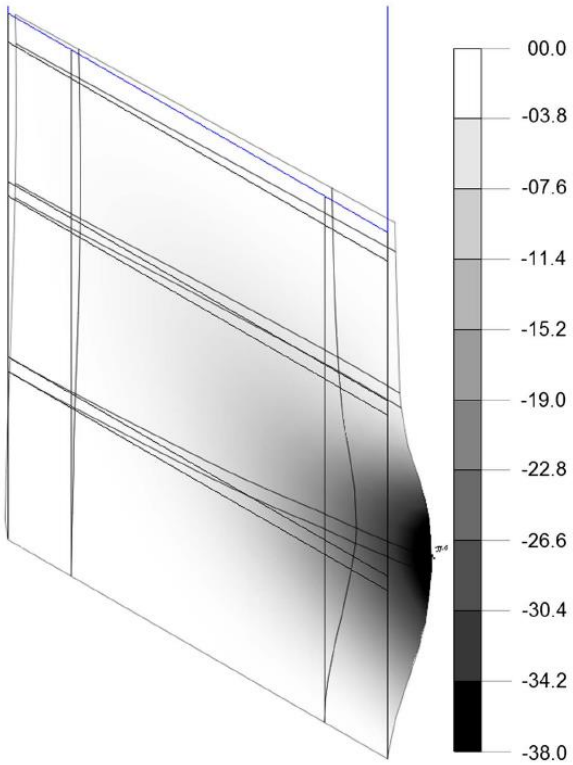

Figure 15. Out-of-plane deformation of the numerical model at 0.0% drift reversing from -2.5% drift (in mm)

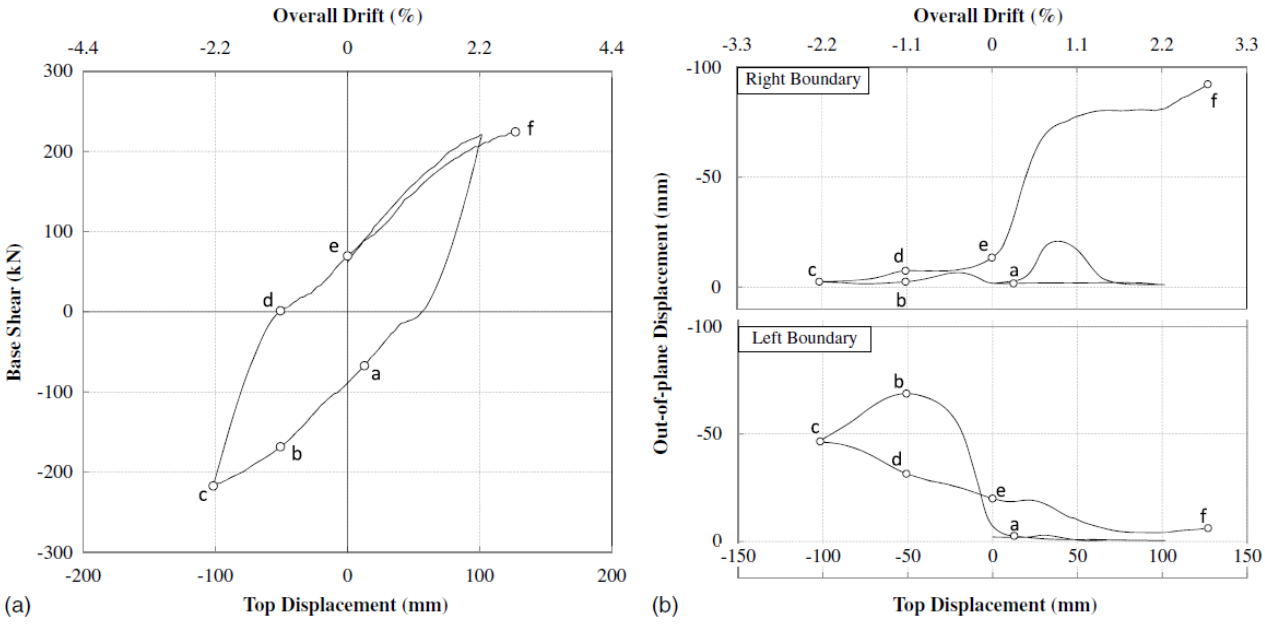

Figure 16. Points corresponding to occurrence of the out-of-plane instability in 101.6mm (4in) cycle: (a) base shear vs top displacement; (b) maximum out-of-plane displacement at boundary zones

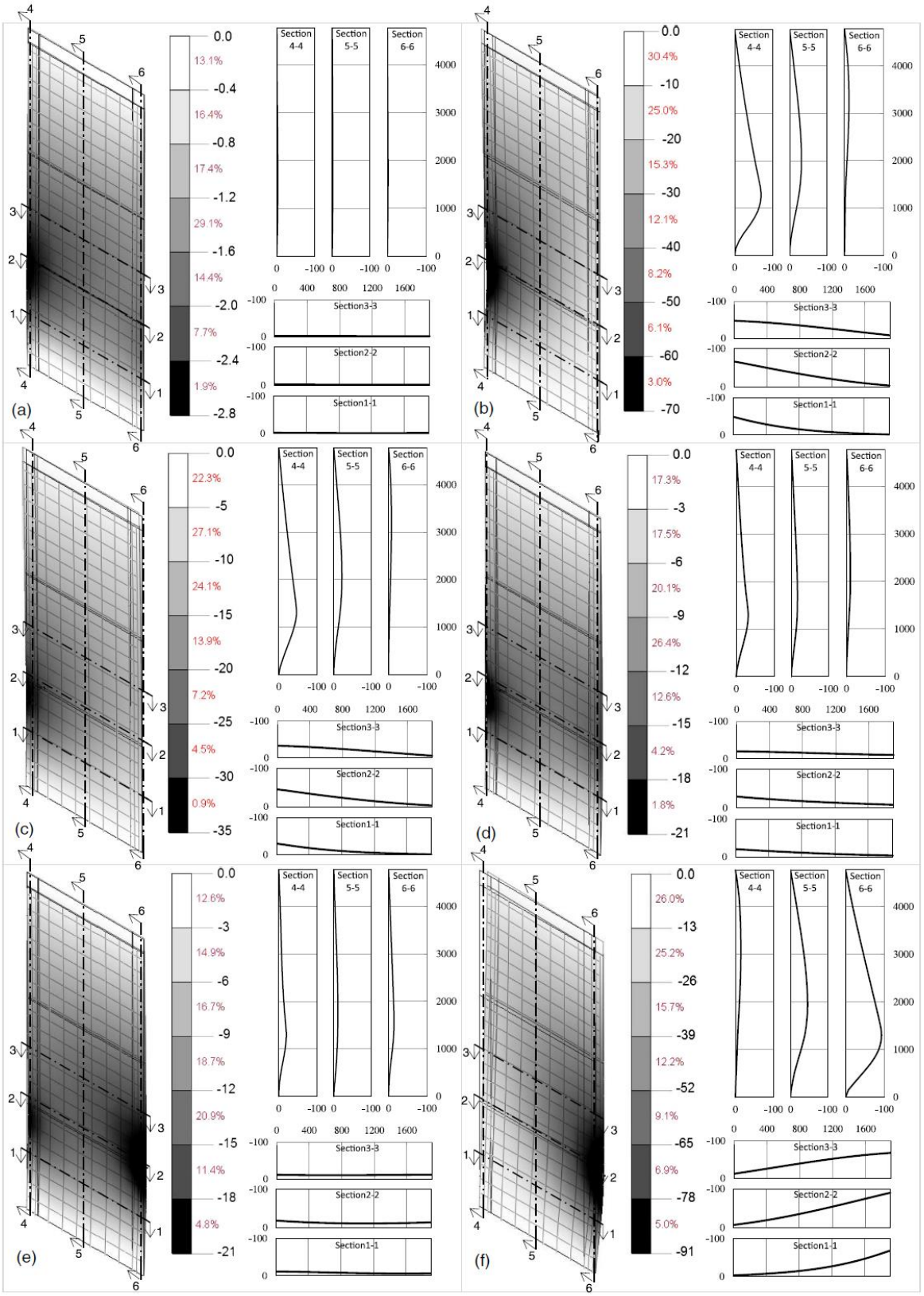

Figure 17. Out-of-plane deformation of the specimen (all dimensions in mm); Figures (a)-(f) correspond respectively to points (a)-(f) in Figure 16

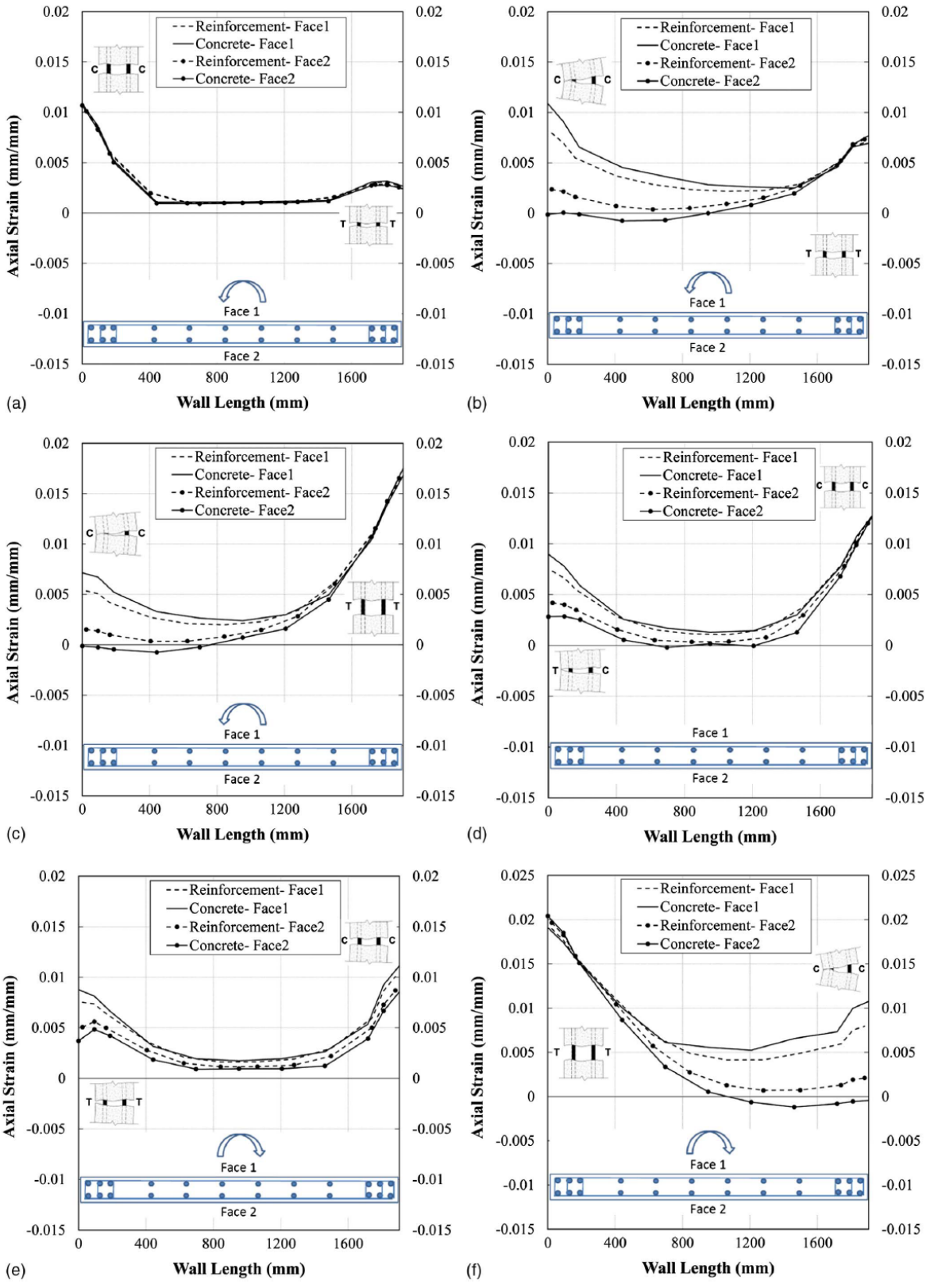

Figure 18. Strain gradient along the wall length: Figures (a)-(f) correspond respectively to points (a)-(f) in Figure 16

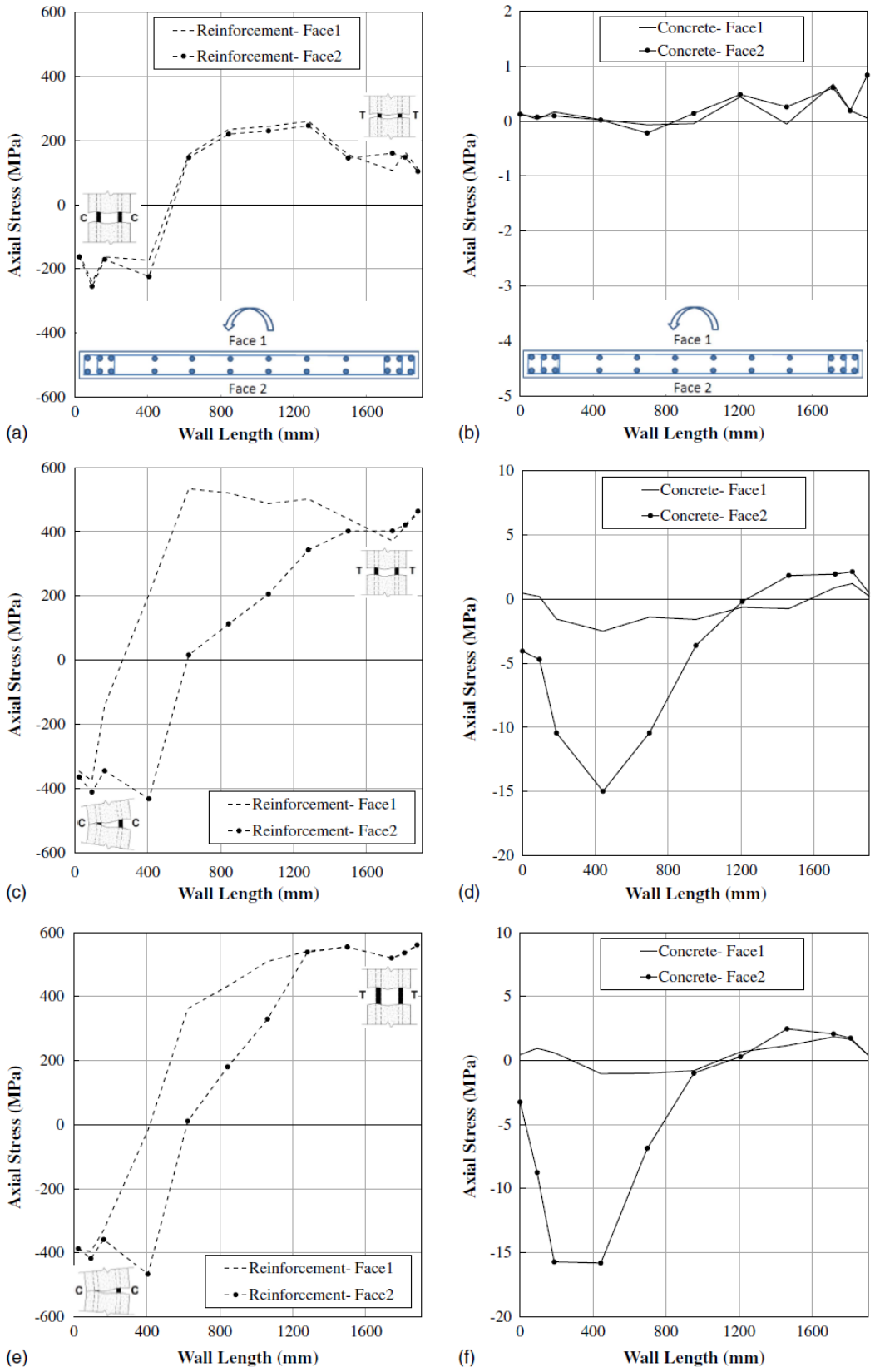

Figure 19. Stress gradients along the length of the wall model (Specimen R2) at Points a–c in Fig. 16: (a) stresses at Point a in reinforcement; (b) stresses at Point a in concrete; (c) stresses at Point b in reinforcement; (d) stresses at Point b in concrete; (e) stresses at Point c in reinforcement; (f) stresses at Point c in concrete

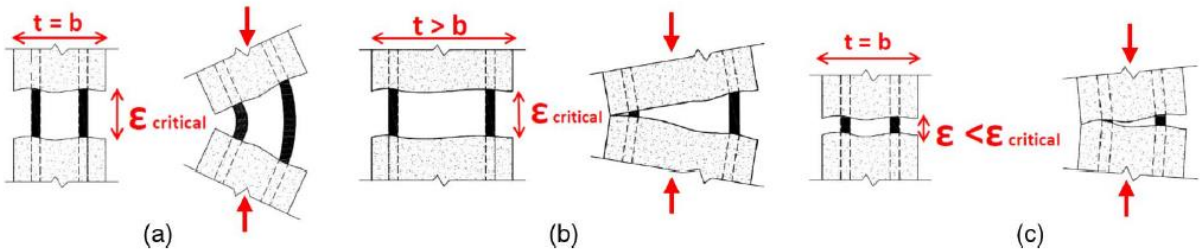

Figure 20. Effects of residual strain and wall thickness on development of out-of-plane instability

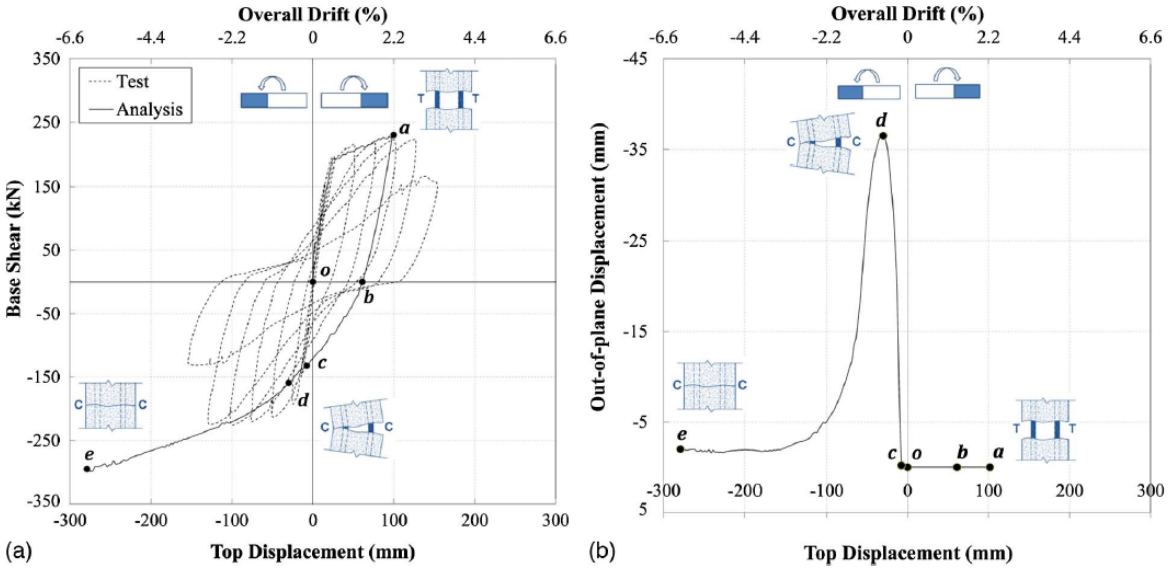

Figure 21. Response of the model: (a) lateral load vs top displacement response and comparison with experimental results; (b) maximum out-of-plane displacement

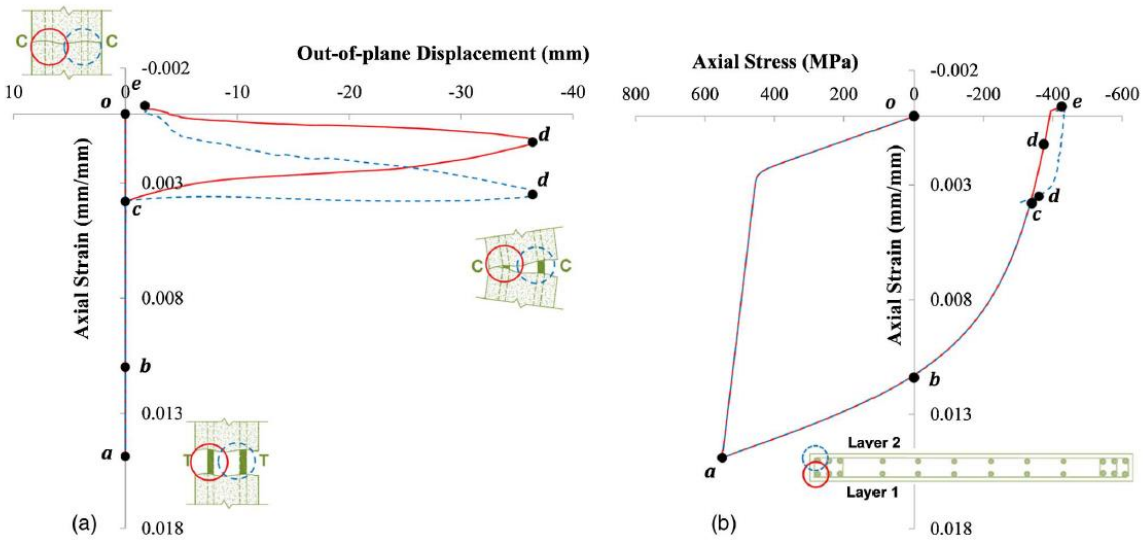

Figure 22. Axial reversed cyclic response of boundary region reinforcement: (a) axial strain versus out-of-plane displacement; and (b) axial strain versus axial stress

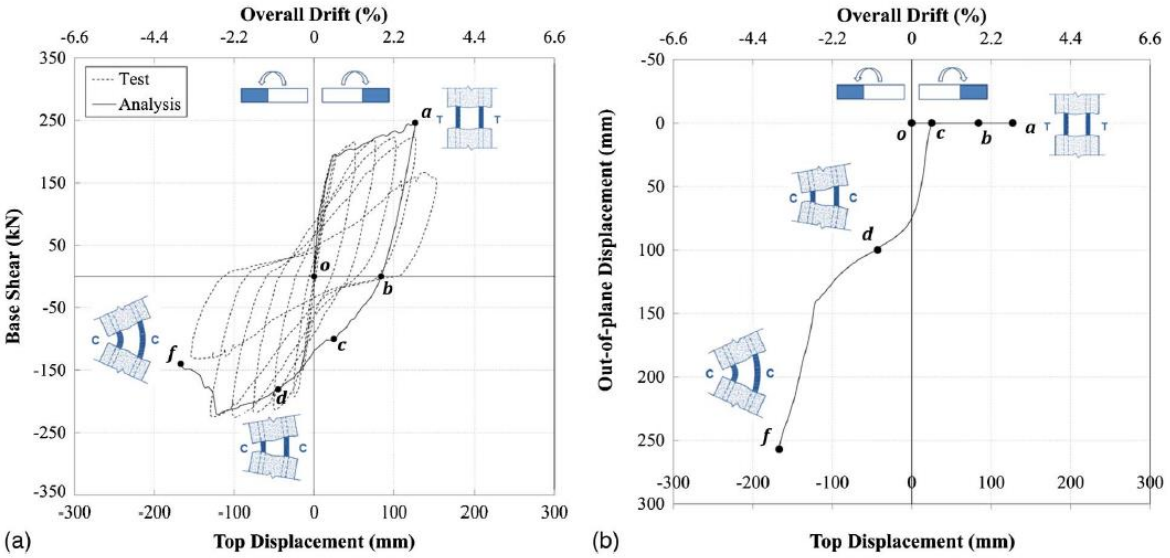

Figure 23. Response of the model: (a) lateral load vs top displacement response; (b) maximum out-of-plane displacement

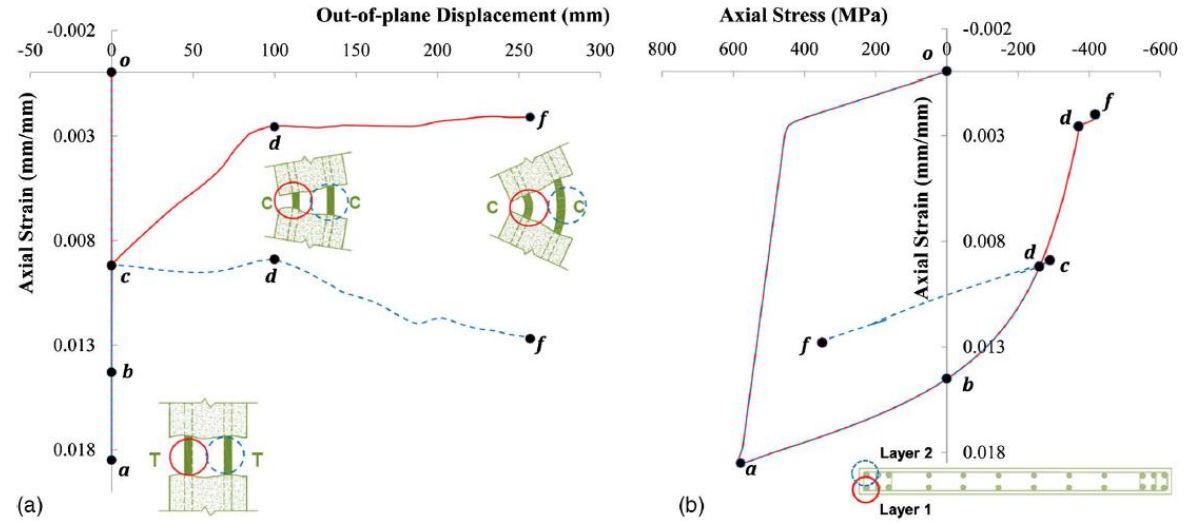

Figure 24. Axial reversed cyclic response of boundary region reinforcement: (a) axial strain versus out-of-plane displacement; and (b) axial strain versus axial stress

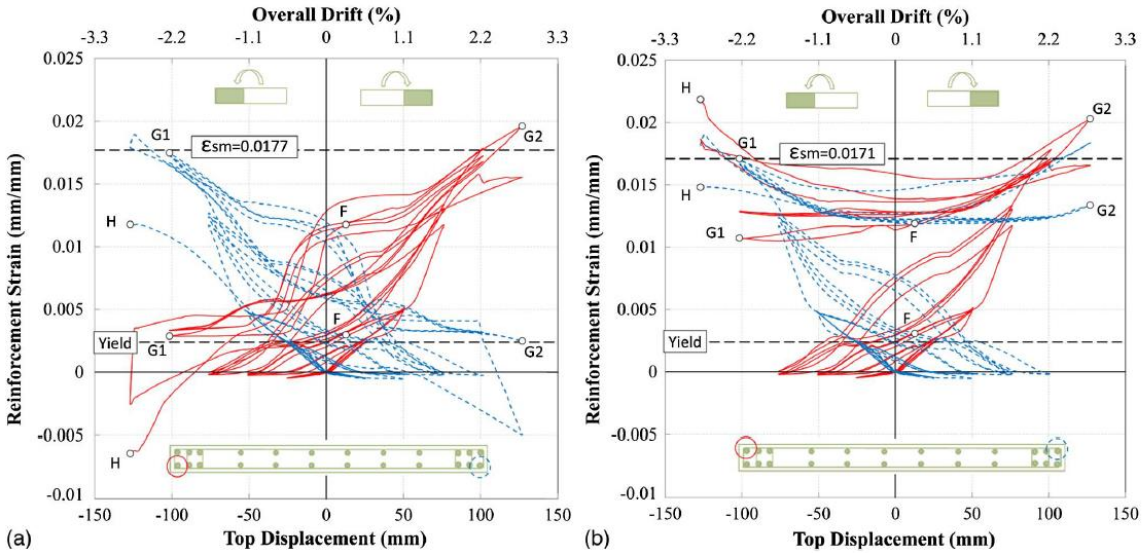

Figure 25. Strain history of the reinforcement at 1.3m above the base

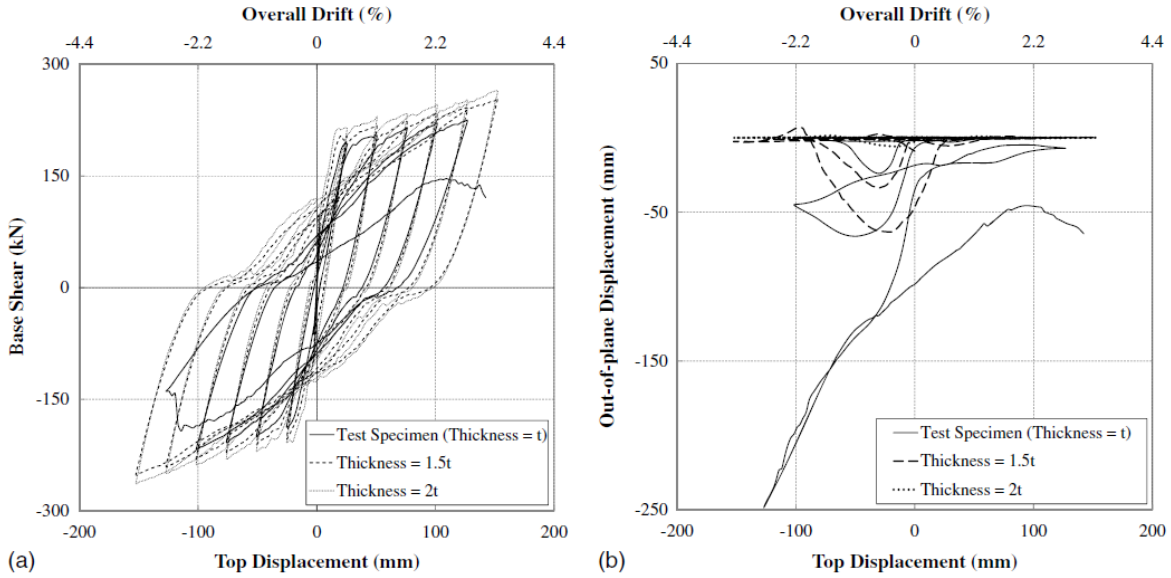

Figure 26. Effect of wall thickness on the model response: (a) lateral load-top displacement response; (b) maximum out-of-plane displacement in the left boundary region

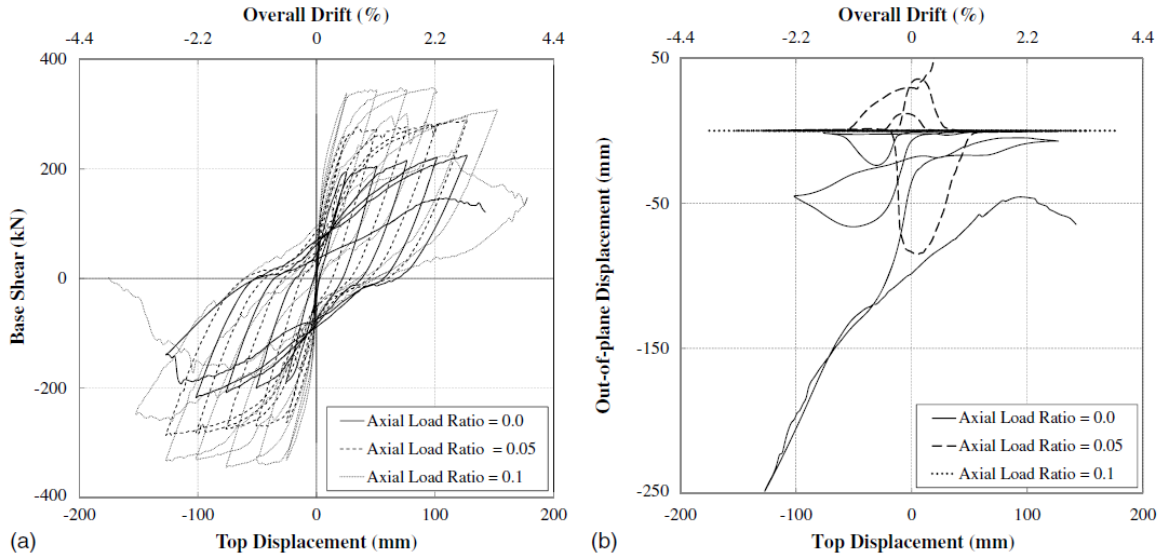

Figure 27. Effect of axial load ratio on the model response: (a) lateral load-top displacement response; (b) maximum out-of-plane displacement in the right boundary region